General Disclaimer

One or more of the Following Statements may affect this Document

- This document has been reproduced from the best copy furnished by the organizational source. It is being released in the interest of making available as much information as possible.

- This document may contain data, which exceeds the sheet parameters. It was furnished in this condition by the organizational source and is the best copy available.

- This document may contain tone-on-tone or color graphs, charts and/or pictures, which have been reproduced in black and white.

- This document is paginated as submitted by the original source.

- Portions of this document are not fully legible due to the historical nature of some of the material. However, it is the best reproduction available from the original submission.

E82-10360
CR-168981

SECRETARIA DE PLANEJAMENTO DA PRESIDÊNCIA DA REPÚBLICA

CONSELHO NACIONAL DE DESENVOLVIMENTO CIENTÍFICO E TECNOLÓGICO

(E82-10360) A STUDY OF ATMOSPHERIC DIFFUSION FROM THE LANDSAT IMAGERY (Instituto de Pesquisas Espaciais, Sao Jose) 58 p HC A04/MF A01 CSCL 04A

N82-26758

G3/43 Unclas 00360

RECEIVED BY
NASA STI FACILITY
DATE: 3-1-82
DCAF NO. 002949
PROCESSED BY
☒ NASA STI FACILITY
☐ ESA - SDS ☐ AIAA

INSTITUTO DE PESQUISAS ESPACIAIS

1. Publication Nº	2. Version	3. Date	5. Distribution
INPE-2284-PRE/060		Dec., 1981	☐ Internal ☒ External ☐ Restricted

4. Origin: DME — Program: RECAT

6. Key words - selected by the author(s)

LANDSAT IMAGERY
ATMOSPHERIC DIFFUSION

7. U.D.C.: 551.510.42:550.3

8. Title: INPE-2284-PRE/060

A STUDY OF ATMOSPHERIC DIFFUSION FROM THE LANDSAT IMAGERY

10. Nº of pages: 57

11. Last page: 54

12. Revised by

Renato Hers

9. Authorship: Y. Viswanadham
J.A. Torsani

Responsible author: Y. Viswanadham

13. Authorized by

Nelson de Jesus Parada
Director

14. Abstract/Notes

Detailed analyses of the Landsat multispectral scanner (MSS) data of the smoke plumes which originated in eastern Cabo Frio (22° 59'S; 42° 02'W) and crossed over into the Atlantic ocean, are presented to illustrate how high-resolution Landsat imagery can aid meteorologists in evaluating specific air pollution events. The eleven Landsat images selected are for different months and years. The results show that diffusion is governed primarily by water and air temperature differences. With colder water, low-level air is very stable and the vertical diffusion is minimal; but water warmer than the air induces vigorous diffusion. The applicability of three empirical methods for determining the horizontal eddy diffusivity coefficient (K_y) in the Gaussian plume formula was evaluated with the estimated standard deviation of the crosswind distribution of material in the plume (σ_y) from the Landsat imagery. The vertical diffusion coefficient (K_z) in stable conditions is estimated using Weinstock's formulation. These results form a data base for use in the development and validation of meso-scale atmospheric diffusion models.

15. Remarks: Submitted to Journal of Geophysical Research - Oceans and Atmospheres.

A STUDY OF ATMOSPHERIC DIFFUSION FROM THE LANDSAT IMAGERY

Y. Viswanadham and J. A. Torsani

Instituto de Pesquisas Espaciais - INPE

Conselho Nacional de Desenvolvimento Científico e Tecnológico - CNPq

12.200 - São José dos Campos, SP, Brazil

ABSTRACT

Detailed analyses of the Landsat multispectral scanner (MSS) data of the smoke plumes which originated in eastern Cabo Frio (22^0 59'S; 42^0 02'W) and crossed over into the Atlantic ocean, are presented to illustrate how high-resolution Landsat imagery can aid meteorologists in evaluating specific air pollution events. The eleven Landsat images selected are for different months and years. Conventional interpretation techniques are applied to analyse the images with a view to arrive at certain plume characteristics. The analysis of the visible smoke plumes revealed that the plume was 130 km long and attained a maximum width of 937 m, 10 km away from the chimney emitting the effluent. The results show that diffusion is governed primarily by water and air temperature differences. With colder water, low-level air is very stable and the vertical diffusion is minimal; but water warmer than the air induces vigorous diffusion. The applicability of three empirical methods for determining the horizontal eddy diffusivity coefficient (K_y) in the Gaussian plume formula was evaluated with the estimated standard deviation of the crosswind distribution of material in the plume (σ_y) from the Landsat imagery. Most consistent estimates for K_y are obtained from the formula based on Taylor's theory of "diffusion by continuous moment". K_y values of about 157.64 $m^2\ s^{-1}$ in quasi-neutral conditions and 48.59 $m^2\ s^{-1}$ in stable conditions are obtained from a plot of σ_y^2 as a function of distance from the source. The vertical diffusion coefficient (K_z) in stable conditions is estimated using Weinstock's formulation. The estimated values of K_z vary from 0.013 $m^2\ s^{-1}$ to 4.42 $m^2\ s^{-1}$ over water surface. The rate of kinetic energy dissipation (ε) is evaluated from the diffusion parameters σ_y and K_y. The ε value ranges from 0.184×10^{-5} $m^2\ s^{-3}$ to 80.2×10^{-5} $m^2\ s^{-3}$ in quasi-neutral and stable stratifications. These results compare well with the previous experimental values obtained over water surfaces by various workers. They form a data base for use in the development and validation of meso-scale atmospheric diffusion models.

1. Introduction

Increased concern for the environmental effects of power plants located on coastal sites and plants proposed for sites offshore has created a need for improved methods to estimate atmospheric diffusion[1] rates over open water. The diffusion properties of the coastal marine atmosphere are unique, principally because the air flows over significantly smoother surfaces, and these conditions have been studied far less than flows over land. That is not to say that the marine boundary layer has not been explored. Because of the difficulty in measuring the instantaneous values of concentration simultaneously at a sufficient number of positions, the observation of relative diffusion has tended to rely mainly on the visual methods, and especially on the observation of the growth and dissipation of puffs of smoke. Earliest examples are contained in discussions of Roberts (1923) and Sutton (1932), in which photographic observations of the growth of antiaircraft shell bursts were used to test theoretical treatments. Later and more extensive series of observations of this type have been reported by Kellogg (1956), and Frenkiel and Katz (1956).

A comprehensive survey of earlier dispersion experiments conducted over oceans and shorelines reported by Prophet (1961) discusses the changing characteristics of flows passing from land to water; a subsequent review by Van der Hoven (1967) sumarizes atmospheric dispersion studies conducted during onshore winds, and classifies various flow regimes as overwater, overland, or in transition from water to land. Perhaps because of the difficulties encountered in conducting meteorological experiments over water,

---

[1] *The more or less interchangeable use of the terms "diffusion" and "dispersion" is intended to convey the idea that the smoke particles in this study, are regarded as having ideal, non-dynamical, fluid attached properties (Gifford, 1957).*

relatively few such studies have been made. Slade (1962) measured air-water temperature differences, mean wind speeds and wind direction fluctuations on the upwind and downwind shores of Chesapeake Bay to obtain estimates of the relative intensities of atmospheric turbulence over land and water. Also, studies of coastal meteorology and diffusion were summarized by Raynor et al. (1975, 1978).

Techniques of utilizing smoke-plume photographs to obtain quantitative estimates of diffusion were first proposed by Richardson (1920) and Roberts (1923), and afterwards applied by Holland (1953), Browne (1961), Culkowski (1961) and Högström (1964). Whitehead et al. (1969) showed that cloud photographs taken during the Apollo 6 mission offered significant meteorological information because of their excellent detail and their adaptability to relative height contouring by stereographic photogrammetry. McLellan (1971) was among the first to attempt to use satellite data to measure anthropogenic pollution by examining the digital brightness values in ATS visible data over the Los Angeles basin. During the Apollo 6 mission, Randerson et al. (1971) have acquired a number of color photographs containing a smoke plume. An earlier analysis of such plumes, utilizing earth satellite photography, was also undertaken by Randerson (1968) who demonstrated that satellite photography could be utilized to study the large-scale transport of atmospheric pollutants.

Lyons and Pease (1973) have presented a series of Landsat-1 satellite images showing that, indeed, smoke plumes from the industrial complex around Chicago - Gary travelled for long distances over water. Lyons (1975a, 1975b) explained that the high-resolution multispectral Landsat-1 image usually will only detect smoke plumes over water surfaces. Griggs (1973) and Mekler et al. (1977) have suggested using Landsat radiance measurements in the visible bands to infer aerosol optical thicknesses and, therefore, the columnar aerosol density over low albedo (water) surfaces. While the technique shows great promise, the Landsat images are made over any given region on the earth only every 9 or 18 days in a narrow strip

180 km wide, and thus do not make it a likely candidate for an operational monitoring system.

The aim of the present study is to find some clues to the problems of diffusion over ocean using Landsat imagery. The cases illustrated here may be considered typical of the diffusion from a continuous point source and the simplest kind of pollution over ocean. They illustrate how satellite data have furthered our knowledge of long-range transport, and indicate the feasibility of estimating the lateral standard deviation, the dissipation rate and the diffusion coefficients of smoke plume from spacecraft.

2. Theoretical considerations

As an introduction to the working formulae, it is useful to consider certain convenient procedures. Consider idealized cases of instantaneous and continuous sources in a homogeneous air stream, with the x-axis in the direction of the mean wind, supposed horizontal, the y-axis across wind and the z-axis vertical. The mean wind is assumed to be constant in space, while the mean components of velocity in the cross-wind and vertical directions are zero. Ideally it is assumed that the instantaneously generated cloud moves in a straight line parallel to the x-axis, expanding in all directions, while the fixed continuous source generates a symmetric plume around the fixed x-axis, with an expanding cross section in the y, z plane. The practical success of explicit diffusion formulae thus depends on the extent to which correct choices of the distribution shape, the lateral standard deviation σ_y and the vertical standard deviation σ_z are contained therein. Comparison with the observations then enable the correctness of the original diffusion treatment to be assessed, and parameters such as diffusion coefficients and intensities of turbulence to be evaluated.

Single-particle diffusion addresses the problem location of a single particle released from a fixed point. The theoretical

foundation was laid down by Taylor (1921) in his historic paper, "Diffusion by Continuous Movement". Relative diffusion concerns the position of two particles released from a single point relative to their mutual center of gravity. The major contribution to the theory of relative diffusion is that of Batchelor (1949, 1952), although Richardson (1926) acknowledged the problem many years earlier. The apparent lateral eddy diffusivity coefficient (K_y) is defined as

$$K_y = \frac{1}{2} \frac{d\sigma_y^2}{dt}, \qquad (1)$$

where t is time. This relationship between the apparent K_y and σ_y along the y-axis was derived by Batchelor (1949). Unlike Fickian diffusion, the scale of plume need not be larger than the scale of turbulence since the K_y in Eq. (1) depends on the standard deviation $\sigma_y(t)$, which according to Taylor's (1921) theorem, depends on the entire energy spectrum. By virtue of Taylor's hypothesis, Eq. (1) becomes

$$K_y = \frac{1}{2} \bar{u} \frac{d\sigma_y^2}{dx}, \qquad (2)$$

where $\bar{u}$ is the mean wind speed along x-axis. Here, it is assumed that Taylor's hypothesis is applicable to the flow with homogeneous turbulence in the lateral at each horizontal plane. For steady state flow, it is no longer necessary to assume the validity of Taylor's hypothesis, and the apparent K_y is defined as in Eq. (2). The apparent K_y depends on the height and the downwind distance; the increase of the lateral mixing with height is due to the increase in the size of eddies, as particles are displaced further away from the boundary. As a consequence of using the apparent K_y, the predicted concentration distribution in the crosswind direction is of Gaussian distribution. This result is consistent with the application of the statistical theory used in the derivation of the Gaussian diffusion model.

Incidentally, the dissipation rate of turbulent energy ε is estimated. Many studies on the turbulent diffusion have been carried out since Richardson (1926), and the following is familiar:

$$K_y \propto \varepsilon^{1/3} \sigma_y^{4/3} \tag{3}$$

where σ_y is the scale of the diffusion process. This 4/3 power relation is that derived from Heisenberg's (1948a, b) treatment of eddy viscosity, and, as found by Richardson over a very wide range of σ_y, much wider in fact than would be expected from the similarity hypotheses and the ideas about the isotropy of the atmospheric turbulence. It may be, however, that very large atmospheric eddies, which certainly are not isotropic (their vertical motions are necessarily small compared with their horizontal motions), tend to a state of restricted isotropy, in the horizontal.

The Gaussian diffusion model has made a significant contribution to diffusion estimates. Gifford (1959, 1968) generalized the Gaussian diffusion model to several simple formulas specially adapted to yield diffusion coefficients directly from photographic measurements of average plume dimensions. Of particular interest in this case are the following two equations for evaluating the lateral eddy diffusivity coefficient K_y:

$$K_y = \frac{\bar{u}\, Y_m^2\, e^{1/3}}{2\, X_t}, \tag{4}$$

$$K_y = \frac{\bar{u}\, Y_m^2}{2\, X_m}, \tag{5}$$

where X_t is the total plume length and X_m is the distance downwind from the source at which the maximum plume width Y_m occurs. Randerson et al. (1971) have also used Eqs. (4) and (5) to estimate K_y from smoke-plume photographs.

Determinations of the vertical variance, σ_z^2, and the corresponding vertical eddy diffusion coefficient, K_z, are dependent on measurements of concentration at different heights and hence are less reliable than those of σ_y^2 and K_y. Lilly et al. (1974) proposed the following expression for K_z in the stratosphere:

$$K_z = \frac{\varepsilon_T}{3\ N^2}, \tag{6}$$

where ε_T is the average rate of kinetic energy dissipation by molecular viscosity and N, the Brunt-Väisälä frequency (s^{-1}). This expression for K_z was based on the assumption that the flux Richardson's number (R_f) is 1/4 and that energy production is locally dissipated. The vertical turbulent diffusion coefficient in a stably stratifield fluid is also derived analytically by Weinstock (1978), i.e.,

$$K_z \simeq 0.81\ \frac{\varepsilon}{N^2}. \tag{7}$$

Since most occurrences of turbulence theoretically should have an inertial subrange for small enough scales, it follows that Eq. (7) might be fairly generally applied to stable atmospheric conditions (Weinstock, 1978). Weinstock's derivation does not require that the flux Richardson number be known or specified. It is seen that Eq. (7) is in approximate agreement with the expression of Lilly et al. (1974) for K_z given by Eq. (6). Eq. (7) gives a larger diffusion coefficient by a factor of 2.4 than Eq. (6). Weinstock (1978) presented a detailed explanation to this fact. He suggested that the smaller value of K_z obtained by Lilly et al. might be attributed to the fact that turbulent fluxes were neglected (i.e., production was assumed to be local). This led to a smaller value of R_f(= 1/4) and a smaller value of K_z. Assuming an inertial range turbulence of the atmosphere, the values of K_z are obtained from Eq. (7) in the present study.

3. Site and weather conditions

The site of Fábrica Nacional de Alcalis (National Chemicals Industry) is located on the east shore of Cabo Frio, about 120 km east of Rio de Janeiro city in the state of Rio de Janeiro, Brazil (Fig. 1). The Cabo Frio area (22° 59'S; 42° 02'W) of eastern Brazil is a flat coastal region bounded north-west by land and the rest by Atlantic ocean. The coast is straight, uncomplicated and typical of much of the northern and southern seaboard from Cabo Frio town. East of Itaipu the ocean is separated from the mainland by a low barrier beach and shallow lacks; water depths increase gradually to about 50 m at 5 km from the shore, approximately.

The height of Fábrica Nacional de Alcalis is 7 m above mean sea level. The Cabo Frio region has a tropical temperature regime with a mean annual temperature 20°C and a high average annual rainfall 1600 mm (WMO, 1975). Particularly during spring and summer months, sea breezes occur on a large percentage of all days in the afternoon, approximately 1200 to 1700 hours of local time. During this period, winds are relatively strong throughout the area. The mean monthly atmospheric mixing heights vary between 870 and 1220 m (Nicolli, 1977).

Weather in the region is subject to variations of the position of the tropical maritime anticyclone with easterly winds blowing on the coast. The cold polar anticyclone in Argentina, by its presence, pushes the tropical maritime high, and the winds back to northeast, north and finally northwest on the approach of the cold front. Then the winds change back to southwest, southeast, as the cold front advances northeastwards. This cycle repeats itself as the cold polar anticyclone, already in low latitudes, degenerates into the tropical maritime anticyclone. From July to December the cycle is quick, and slows down from January to June since the cold airmass is not strong enough to push the tropical anticyclone into the ocean. The effect is a seasonal one with a dominance of easterlies or northeasterlies during summer and fall, and southwesterlies or

westerlies during winter and spring. The Cabo Frio region is noted for its upwelling which has a great biological importance in the production and variation of fish "Sardinella aurita" (Silva, 1971).

4. Data sets and processing

Emission parameters and meteorological data

The visible smoke plumes obtained from the Landsat imagery are emitted by the Fábrica Nacional de Alcalis of Brazil. The emission parameters from the 76 m stack height of the industry are: gas flow rate 200 $m^3\ s^{-1}$; exit gas speed 7 $m\ s^{-1}$; gas composition by volume: 47% of water vapor, 41% of N_2, 10% of O_2, 2% of CO_2 and traces of CO, NO_x, SO_2, Mg, $MgSO_4$ and NaCl (Companhia Nacional de Alcalis, 1979).

The meteorology of urban coastal regions generally differs considerably from the features of inland urban areas. The mesoscale meteorological conditions existing during the period (1975-1978) of interest could be approximated from available data of two agencies. Due to the lack of adequate meteorological measurements for inland and oceanic areas of the Cabo Frio region at the time of Landsat imagery, the upper air observations data were taken from the international airport of Galeão, Rio de Janeiro, Brasil (Força Aérea Brasileira, 1974-1978). Surface weather conditions, i.e., wind speed and prominent wind direction at 10 m height, screen dry - and wet - bulb temperatures, solar insolation and cloud cover for 6 hrs intervals starting from mid-night are available at a weather station (Instituto Nacional de Meteorologia, 1968-1978) very close to the industry. The radiosonde soundings for each Landsat imagery were plotted for the 3-day period (one day before and one day after the passage of satellite) along with the surface data. Then, the interpolated mean wind speed was obtained at 76 m stack height level. In Table 1, the base and top of the inversion heights are presented along with other details.

Satellite data

The application of Landsat imagery in the earth sciences is steadily gaining favour. It is particularly useful for the study of areas where accurate ground truth is difficut to obtain. The Instituto de Pesquisas Espaciais (INPE), Brazil, has issued maps with path and row number of the area over which they can receive Landsat satellite multispectral scanning (MSS) data in real time. The classification of the four channel low-resolution scene was carried out on an interactive display system GE - Image 100 (General Eletric Company, 1975). The primary function of the Image 100 system is to extract thematic information from multispectral imagery. A secondary function is as an image enhancement system. Using this system, Landsat/MSS data were processed digitally to perform image rectification and classification. In order to derive accuracy information, a verification procedure based upon a systematic random sampling scheme was applied to the digitally processed classification Landsat and terrain data sets. Examples of processed imagery are presented in section 4 of General Electric Company (1974) in order to illustrate practical application of Image 100.

Eleven Landsat images of the Cabo Frio region were obtained at an average local time between 0830 to 0930 hrs, with a view to arrive at certain smoke plume characteristics. They were selected for analysis on the basis of having a minimum of fair data quality in bands 4, 5, 6 and 7, and no interference from clouds over the study site (Table 1). The thematically classified Landsat data produced by digitizing 1:100,000 scale maps appear to be suitable for portraying elevations for the present study. The images slected on the basis of acceptable quality were found to coincide with the local time of radiosonde ascents at Galeão Airport, approximately.

Computer compatible tapes and interactive multispectral analysis systems allow individual picture elements to be analyzed and displayed using statistical and mathematical processing functions. The

enhanced images were displayed in the video equipment and photographed with Kodak colour II - 100 ASA - 35 mm negative film and also with Ektachrome - 64 ASA - 35 mm slide film. The photographed films were used for subsequent enlargement to the size of 45.5 x 70.0 cm on a transparent paper (Fig. 2), and measurements were made of the plume dimensions with the aid of an equipment 3M Brand, 201 Dry Silver Reader Printer.

The crosswind dimension of a smoke plume is conventionally represented either by the width between positions at which concentration falls to a given fraction (usually one-tenth) of the central value (Fig. 2). When the distribution is of Gaussian form and the fraction adopted in specifying smoke plume width ($2\ Y_0$) is one-tenth, the standard deviation of the crosswind displacement of the material σ_y, in practice defined by Pasquill (1961) and Gifford (1961), is

$$\sigma_y = 2\ Y_0/4.3 \quad . \tag{8}$$

Estimates of σ_y were obtained from measurements of visible plume width on all usable photographs with known geometric relationship (8). These smoke plume spread measurements can be converted into useful information regarding over-water mesoscale diffusion of pollutants.

5. Results

Observations of plume behavior

The foregoing classification of smoke plumes from Landsat imagery provides a useful approach to the broad specification of diffusion in terms of general weather conditions. They may be used in assessing the quality of diffusion effects on particular occasions. However, apart from the qualitative nature of the results, there are numbers of limitations in the present approach due to the meteorological data sets, topography and climatology of the site. For

the achievement of quantitative and reliable estimates of diffusion it is necessary to have accurate simultaneous turbulence measurements in space and time. To be exact, the characteristic variation of wind structure with height above ground should be taken into account. But the over-all effect of mesoscale motions would most likely be an increased diffusion over water. In Table 1, reference number of Landsat image cases, various meteorological parameters, heights of inversion base and top, and the gradient Richardson number are presented for a qualitative description of the smoke plumes. A deep surface super-adiabatic layer failed to form, however, due to the relatively weak sunshine. The Richardson gradient numbers which were computed by taking temperature differences below 80 m level of the radiosonde show that quasi-neutral and stable conditions predominated. The radiosonde data did detect surface inversions below 900 m and also elevated ones beginning about 1300 m, extending to about 2500 m, in some cases (Table 1).

Figs. 3-13 are portions of the Landsat images taken at approximately 1130 to 1205 GMT during the period April 1975 to July 1978 for the Cabo Frio region. These figures illustrate typical phenomena which occur in a coastal transition zone during a period of quasi-neutral and stable offshore air flow over a water surface. Mixing depths over the water are greatly restricted and turbulence values are small. If one compares the slopes of the plume axes on different traverses, one can see a great deal of variance. For much of the days the plumes appeared approximately in NNE direction. The prime cause for such variations is the directional shear of the wind which can be a rapidly changing parameter (Högström, 1964; Smith, 1965). In most of the cases, the winds oscillated very little at 80 m altitudes and there was comparatively a small variation of directional shear. Wind speeds at plume levels approached approximately 2 to 11 m s^{-1} during the late morning, but gradually diminished to less than 4 m s^{-1} by late afternoon. From Figs. 3-13, one gets the distinct impression that the turbulent plume rising from the stack is being literally blown over in response to increasing wind speed. Also, plume trapping

is a cammon diffusion penomenon that occurs over land, water in transitional zones, such as coastlines.

Saffman (1962) and Csanady (1969) have developed theories for diffusion from an instantaneous point source in winds enhibiting speed and directional shear. Csanady (1972) found that the lateral spread of a pollutant plume may be dominated by directional shear when the pollutant has mixed sufficiently within the shear layer. In general, the present results (Figs. 3-13) agree in their general features with those obtained in the theoretical studies by Saffman (1962), Högström (1964), Smith (1965) and Csanady (1969), and in a numerical study by Tyldesley and Wallington (1965).

From Figs. 3-13, we can see that wind shear is practically always present, and acts to elongate a smoke cloud and tears it apart. Often, this effect is so strong that it tends to mask the small-scale effect of diffusion. It must be emphasized, however, that wind shear and eddies due to turbulence are really indistinguishable except for their difference in scale, and it is probably impossible to draw a line of demarcation between the two. This is done in practice to simplify the analysis, and an arbitrary assumption has been made to the effect that diffusion acts to spread the smoke plume radially, while shear acts to alongate it (Kellogg, 1956). Actually, this means that we are eliminating from consideration the effects of those eddies which are larger than the size of the smoke cloud, and calling their effect "shear". The radial growth of the smoke cloud size does not depend on wind shear or wind speed, but does show an increase with height (Fig. 10). However, the vertical mass growth shows a decrease with increasing stability (Figs. 7, 13). This may be interpreted in terms of the concept of the well known Reynold's stress, which says, in effect, that eddy stress is proportional to the vertical transport of momentum, and this is given by $\rho\overline{u'w'}$, where u' and w' are associated horizontal and vertical components of eddy velocity, and ρ is the air density. Clearly, the growth of the smoke cloud at first will be proportional to these eddy velocities; and, so,

it may be said that the vertical transport of momentum is proportional to the mass growth; and this, in turn, should be inversely proportional to the stability of the atmosphere $\frac{g}{\theta}\frac{\partial\theta}{\partial z}$, which will tend to suppress the vertical transport of any property. Thus, the above argument suggests why one would expect the inverse relationship between these two parameters, as displayed very markeddly in Figs. 7 and 13.

An important consideration is the choice of the appropriate Landsat spectral band to provide optimum discrimination of a particular plume against the underlying surface, in this case water. Lyons and Pease (1973) have presented a critical discussion about the combined effects of high water spectral albedo and low inherent image constrast. They have also presented other theoretical considerations regarding the poorest plume discrimination above a water surface. The plume will be most visible on the photograph when the difference between the optical density of the plume image and the optical density of the ocean-surface image is greatest (e.g., Figs. 3, 5, 6, 7, 13). A consequence of the greater transparency of water in the blue and green portion of the spectrum occurs in the case of shallow water, where reflection from the deep ocean layers may funther increase the value of the ocean surface albedo and limit the ability to detect pollution plumes (e.g., Figs. 8, 9, 12). It should be noted that due to the various degradations involved both in making the photographic print and in publication, the plumes (Figs. 8, 9, 12) do not appear as clear as in the original 35 mm negatives. The prints were also photographically dodged to maximize details over water.

Further complications arise when the assumptions of "steady-state" plumes are employed. Rapid variations in wind vectors with space and time are characteristic of the coastal environment. Not only does the specification of diffusion become difficult, but pollutant transport (as determined by the orientation of the plume centerline) is found to be exceedingly complex. Figs. 3, 4, 5, 6, 8, 9, 12, and 13 show that the turbulent intensities over water surfaces

frequently appear to be lower than over land because of (a) reduced aerodynamic surface roughness, and (b) buoyant festering forces resulting from airmass stabilization during periods of warm air advection over colder waters. Thus, both the mechanical and thermal components of turbulence can be affected, and diffusion rates diminished. On the other hand, during periods of advection of colder and/or drier air over water, active thermal convection patterns can generate intense turbulence on several scales (see cumulus clouds on the left side of Fig. 5). Furthermore, since moist air is lighter than dry air at the same dry bulb temperature, during periods of significant evaporation buoyant forces can also be more intense than equivalent conditions over land. This last matter has been little explored.

Figs. 5 and 7 are quite typical in nature. Rows of cumulus clouds were formed a few kilometers offshore. What is relevant here is that the airmass in question has been transformed from stable (or perhaps near neutral) stratification over land to an ever deepening layer of neutral to slightly superadiabatic lapse in a relatively short distance from the shore line. At the surface, Phillips (1972) has also found that approximately 50% of the total air temperature modification takes place within the first ten minutes of over water fetch. In the vertical, the air mass modification is more complex. From Table 1, it can be noted that there was a higher level inversion on June 23, 1976. Generally, this is a synoptic subsidence inversion. In a series of aircraft measurements, Lenschow (1973) illustrated that an elevated inversion is usually present in the offshore flowing air stream. The inversion surface over the lake is usually severely altered, generally increasing with height with downwind fetch, capping a mixed layer. Lavoie's (1972) numerical model of lake effect storms shows that the inversion deformation over the lake and for many tens of kilometers inland can be a spatially complex pattern of quite significant magnitude. While for the most part the inversion base is increased to greater heights, some results suggest that it may actually decrease several hundred meters in height over

the upwind shoreline regions. This is in response to the intense mesoscale divergence in the low level flow found over the upwind shoreline region. Thus, estimating mixing depths is and around, and even upwind of a Great Lakes shoreline during these lake effect storms can be more complicated than one might expect. Of course, the same phenomena occur over oceans on a much larger scale. One merely need glance at any satellite photograph taken during winter (e.g., Fig. 7) to see the convective cloud lines over the oceans whenever cold air streams over warner air (Tsuchiya and Fujita, 1967).

In Figs. 5, 6, 7, 12 and 13, a bend in the plume axis appears. Probably, this is the result of a change in the marine boundary layer wind direction associated with the meander phenomena. In the atmosphere there is an existence of the shorter term fluctuations of a period of less than one hour. These are extremely important in terms of producing plume meander, which, it is felt, causes considerable oscillation of the plume about its smoothed azimuth. The effect of such higher frequency motions is to cause the plume axis not to lie along a straight line, and also to result in considerable lateral fluctuations of the location of the fumigation spot. It is not easy to treat these small scale fluctuations in a direct manner without having accurate turbulent measurements. The great initial turbulence within the plumes is such that active diffusion predominates over passive for several kilometers downwind. The strong thermal stability appears more effective in damping the vertical turbulence components than the horizontal (Figs. 7, 12, 13). During more stable conditions (Figs. 7, 12, 13), the plumes were often very narrow and cohesive, staying close to the water for distance of 80 km or more, even with wind speeds on the order of 4 - 5 m s^{-1}. Fig. 7 shows that the diffusive capacity of the air into which a pollutant is emitted is limited in the vertical by a more stable layer above.

Figs. 3, 7 and 9 show a break-up in the plumes. This is related to wind shifts in the marine boundary layer. In the case of

n = 7 (Fig. 9), a weak inversion has been observed. In fact, this weaker conduction inversion in the offshore flow has resulted into a least defined plume (Fig. 9). From Figs. 3,4,6,8,9,12 and 13, it must be noticed that as long as the air over the ocean is warner than the underlying water surface, no penetrative convection will occur during the many hours of cross-ocean flow. Also, skies were clear. Thus the layers above 76 m (where the stack plumes reside) did not show as marked a difference in plume diffusion characteristics as might be expected. Figs. 7, 10 and 11 show penetrative convection phenomena in which the ocean surface temperature is greater than air temperature. In such situations (Figs. 10, 11), the complex interactions of the entrainment of environmental air into the plume by its internal turbulence, and detrainment of plume matter into the atmosphere by its turbulence created difficulties in determing the boundary contours of plume and estimation of σ_y values (Table 2). In Fig. 10, it can be seen that in the vertical the plume has been thoroughly mixed. Vigorous convection had built up to a distance of 8 km just SSW wards of the rushing wind. An interesting feature of Fig. 10 is the extrusion of plume over the ocean. This suggests that, at least for short periods of time, turbulence is a parameter that can be advected with mesoscale airflow.

Evaluation of diffusion parameters

As suggested in the introduction, the phenomenon of plume spread can be quite complex unless some simplifications can be made by careful scrutiny of the physics of the problem. Therefore, in this section, important deductions will be made from the Landsat imagery of smoke plumes and established physical laws of fluid mechanics. The Landsat images have been characterized by a gradient Richardson number (RI) computed from radiosonde and surface observations (Table 1). The RI values given in Table 1 are approximate due to the extrapolation involved in the data sets. However, on the basis of RI values, we classified the Landsat images into quasi-neutral cases (i.e., n = 1, 2, 3, 4, 6, 7, 9) and stable cases (i.e., n = 5, 8, 10, 11).

Measurements of the plume geometry (such as Fig. 1) provide estimate of lateral standard deviation σ_y which was associated with the plume's diffusion in downwind distance (see section 4). The estimates of σ_y from eleven Landsat image cases (Figs. 3-13), and calculated values of lateral eddy diffusivity coefficient (K_y) from Eq. (2) are summarized in Table 2. In every case the same corresponding 76 m height wind speed is used at different downwind distances to calculate K_y values. Mean values of σ_y and K_y for each case are given in the last column of Table 2. The values of K_y are also estimated using the information from the Landsat imagery data sets in Eqs. (4) and (5), and they are presented in the 7th and 8th columns of Table 3 as $(K_y)_4$ and $(K_y)_5$, respectively. Mean values of K_y from Table 2 are also presented in the 9th column of Table 3 as $(K_y)_2$. The ratios $(K_y)_5/(K_y)_4$ and $(K_y)_2/(K_y)_4$ are included in the 10th and 11th columns of the same table, respectively.

In Table 2, for cases n = 1, 6 and 8, we did not estimate σ_y values for long distances due to difficulty in tracing the boundaries of the smoke plumes. From Table 2, it can be seen that the estimated σ_y values over water are smaller than over land for equivalent thermal stabilities. In the previous section, we have explained the reasons for the restricted lateral spread of smoke plumes over water surfaces. The examples given are an indication of the variability of diffusion even when the overall conditions of flow appear to be in an approximately steady state. The major problem in interpretation of diffusion experiments, familiar to all works in this field, is the great variability of the observed data. In Table 2, values of K_y estimated from Eq. (2) are more consistent and they do not show any abnormal and brusque changes with downwind distance.

Table 3 shows the large differences in K_y from three empirical methods (i.e., Eqs. (2), (4), (5)). Eq. (5) gives significantly larger values of K_y in both quasi-neutral and stable conditions. To determine more clearly the applicability of the three methods for estimating K_y in the Gaussian plume formula, we examined

the ratios of $(K_y)_5/(K_y)_4$ and $(K_y)_2/(K_y)_4$. From the ratio of $(K_y)_5/(K_y)_4$, we can say that $(K_y)_5$ is 3 to 19 times greater than $(K_y)_4$. The last column of Table 3 shows that the ratio $(K_y)_2/(K_y)_4$ is sufficiently close to unity in some cases. Eq. (2) overestimates the values of K_y in comparison with Eq. (4) in more stable conditions, whereas it underestimates in more unstable conditions.

The major difficulties encountered in the application of Eqs. (4) and (5) are the correct estimation of the parameters X_m and Y_m from the Landsat imagery. Of course it is understood that other hypothetical distributions of plume particulate density analysis could also present difficulties in choosing correct X_m and Y_m values. But the capability to determine absolute densities has not yet been validated experimentally, except in the case of lidar technique. These input parameters would in effect create abrupt changes in K_y values. Fortunately, there is less difficulty in the determination of the total plume length (X_t) from the Landsat images. Eq. (4) contains only one approximately estimated parameter Y_m, whereas Eq. (5) involves two parameters X_m and Y_m. Therefore, the estimated K_y values from Eq. (5) are more erratic compared to results from Eq. (4). From Tables 2 and 3, we might conclude that Eqs. (2) and (4) give more realistic values for K_y. In addition, for practical purposes, Eq. (2) gives much better results than Eq. (4) if we have correct estimates of σ_y with downwind distance. The calculations indicate that the values of K_y vary from 20 to 5×10^3 m^2 s^{-1} over the Atlantic ocean. The K_y values increase in unstable conditions and they decrease rapidly in stable conditions.

The rate of kinetic energy dissipation ϵ by viscous processes can be regarded as a good indicator of the strength of turbulence. With the aid of certain approximations, the Landsat data sets can be used to make estimates of ϵ in all eleven cases, and the vertical eddy diffusion coefficient K_z in stable case only. Thus, we assumed an isotropic turbulence and inertial range spectrum to estimate ϵ and K_z from Eqs. (3) and (7), respectively. The results are

shown in Table 4 together with other parameters. These values of ε and K_z show the weaker mixing processes in the marine boundary layer. The mean ε values show how sensitive the thermal inertial boundary layer can be to changes in wind, insolation, etc. They must be regarded as tentative, due to the subjective nature of the identification of turbulence categories, and the diverse sources used in computations. There are methods to estimate ε from turbulent measurements. It is not known which estimate of energy dissipation is more reliable.

Although one might expect some values for the parameters (ε, K_y and K_z), a check with actual measurements is more important. Since 1948, many more observations have been available, mainly based on improved techniques of measuring turbulent parameters. We have summarized results of ε, K_y and K_z from each of 40 available publications in Table 5. Most of these are experimental; a few identified are merely discussions or reviews of the general outlook on this subject; but they have been included and given equal weight with others. Note that the reported values of ε, K_y, and K_z in Table 5 are directly comparable with our results in Table 4.

The values we have obtained for ε (Table 4) are consistent with the presented values in Table 5 for water surfaces. The mean values presented in Table 4 for K_y compare well with the 5th column of Table 5. But in four cases (in Table 4, for n = 2, 4, 6, 7) we got higher values for K_y than the maximum value of 100 $m^2\ s^{-1}$ in Table 5. The estimated values of K_z range from a maximum of 3.417 $m^2\ s^{-1}$ to a minimum of 0.013 $m^2\ s^{-1}$ for the data shown in Table 4. These results agree well with most of the values presented for K_z in the last column of Table 5. Lilly et al. (1974) have showed that the ε and K_z are subjected to large variations with underlying surface characteristics, height, latitude and season. Also, the measurements over water are difficult because the spectra extend to very small scales.

Over water, while the surface roughness tends to be more nearly uniform than one could find at land sites, sharp variations in water surface temperatures, especially in near shore region, can make the interpretation of data exceedingly difficult. Furthermore, during periods of offshore flow, intense air mass modification occurs. Thus, as air flows from land to cold water, not only does the boundary temperature change, but the value of the eddy conductivity begins to drop by at least an order of magnitude. There is a destructuction of the mechanism involved in creating such high K_z values over land, since much of the vertical eddy transport probably results from penetrative convection acting over and above the effect of mechanical turbulence. It is this convective component that disappears very rapidly with fetch. The drop in K_z from around 10 to 10^{-1} m^2 s^{-1} (or less) probably occurs within the first few kilometers. Thus, the mathematical necessity of postulating a constant small value of eddy conductivity for the entire fetch is not too serious a problem. The air's vertical diffusion rates should indeed be low in such an environment. There is little or no quantitative information on fetch, wind duration, sea state, etc., with which we can categorize σ_y in the present analysis. Their effects (if any) remain obscure in the data scatter of individual data sets (see Table 2) and of overall mean values (see Table 4). In summary, the present data sets give evidence that the average vertical diffusion in the lower troposphere is somewhat lower in the stable marine boundary layer. On the other hand, the vertical diffusion coefficients of smaller magnitude compared to ours are found appropriate when the quasi-horizontal process are explicitly represented in the global atmosphere (Lilly et al., 1974).

In Fig. 14, the individual maximum Y_m values from Table 3 are plotted against the wind speed at a stack height of 76 m, from which it is seen that there is no marked systematic variation with wind speed. The dispersion parameter σ_y^2 obtained from Landsat imagery is plotted in Figs. 15 and 16 as a function of downwind distance from the source. In Figs. 15 and 16, the straight lines estimated by eye

fit the points on log-linear paper quite well. Still, there is a considerable scatter about the line. There seems to be little doubt that much of the observed variability was due to inherent properties of the field of flow, including the presence of large-scale horizontal eddy motion which produced meandering and distortion of the plume on some occasions. A part of scatter may be attributed to the technique used in estimating σ_y. It is interesting to note that the σ_y^2 values can indeed be used to calculate average lateral diffusion coefficient in quasi-neutral and stable conditions. The coefficients are then estimated to be 157.64 $m^2\ s^{-1}$ and 48.59 $m^2\ s^{-1}$ for quasi-neutral and stable stratifications, respectively with the average wind speed being, respectively, taken as 5.63 $m\ s^{-1}$ and 4.43 $m\ s^{-1}$ (Figs. 15,16).

It is not possible, from the data sets, to establish any clear definite relationship between σ_y and stability. On the other hand, the estimated values of K_y show a strong dependence on the stack height wind speed. Figs. 17a and 17b show K_y as a function of wind speed in quasi-neutral and stable conditions, respectively. On these figures, the lines are obtained on the basis of trail and error method. The lines correspond to K_y increasing as $U^{1.3}$ and $U^{0.85}$ in quasi-neutral and stable conditions, respectively. In both stabilities, K_y increases with the stack height wind speed. From Figs. 17a and 17b, it can be seen that K_y increases more rapidly in quasi-neutral stability than in stable conditions.

There are several possible sources of error in the above computations. Acceptable erros would have been encountered in all instances in any case because of satellite position in relation to the study area, and the size of an individual grid cell compared to the magnitude of possible error (Ernest, 1975; Ernest and Lyons, 1974). Some error may arise from assuming an inertial range spectrum to compute dissipation rate. Also, the vertical, lateral and longitudinal turbulence differed substantially from the assumption of isotropic turbulence. If the lateral component alone were used, as is done in

the present study, Table 4 shows that the values of K_z would be larger by a certain factor. There are no direct atmospheric data against which to test these predictions.

6. Concluding remarks

An analysis of the smoke plumes from a Landsat imagery of the Cabo Frio region has been described. The eleven images selected were of different months and years. These provided intimate descriptions of transport paths and dispersion processes of the smoke plumes over an ocean area. The lateral standard deviation was selected as a measure of plume width and estimated from the plume geometry. Examination of the data sets shows that plume behavior is highly dependent on the stability of low-level air over the ocean. During the warm season, when well mixed air flows over a relatively colder water surface, intense stabilization occurs. It was to be anticipated that the existence of a strong inversion in the temperature profile at some level would decisively halt the upward spread of the particles by convection, and also that in the absence of convection, even without marked stability, the vertical spread would be very slow. This results in concentrated plumes at appreciable long distances over the ocean from the source. However, small changes in wind direction and meander of the plume disturb the plume geometry. It is somewhat uncertain, however, what the effect of meander becomes in the extremely stable flows.

With three empirical methods, the K_y values were evaluated from plume dimensions. Calculations of K_y yielded values ranging from 20 to 5×10^3 m^2 s^{-1} in quasi-neutral and stable conditions. A K_y value of about 157.64 m^2 s^{-1} in quasi-neutral and 48.59 m^2 s^{-1} in stable conditions were obtained from a plot of σ_y^2 as a function of distance from the source. Most consistent estimates for K_y were obtained from Eq. (2). The values of ε have been estimated over water from σ_y and K_y values. The values of K_z were also estimated in stable conditions from ε and N. They range from 0.013 m^2 s^{-1} to

4.42 m^2 s^{-1}. These results compare very well with previous experimental results over water surfaces. At the present stage, the understanding and generalization of data such as those shown in Fig. 14 are hindered by the lack of a satisfactory theoretical framework.

The data described in the present study are isolated examples from which only tentative and rather qualitative deductions are made. Much more data would be required to establish a relation, but this first indication is at least a pointer to the practical analysis of horizontal diffusion. Because of logistic and financial constraints only data from the Landsat system were examined. With an observation frequency of once per 18 days, the data sample is likely to be small indeed. Unfortunately, in many impact statements, due to pressures which are entirely understandable, data from the nearest national weather service office are used in preparing calculations. Thus, the most critical conditions might often be missed. There are probably more important differences in mesoscale climate in the 200 km east of the Cabo Frio region.

Unfortunately, the various aspects of the problem are so diverse that a good synthesis is not yet possible. Yet it was felt that in the long run, it would be benificial to delve into some of the details surrounding the various case studies. We will present in future publications our studies of the simplest case, diffusion over water, complicated only by the fact of varying water surface temperatures or the intense modification which occurs when air crosses the shoreline to traverse water of differing temperature. We will also discuss the basis of mesometeorological systems over water inasmuch as diffusion (and transport) in intimately intermingled with atmospheric behavior on the mesoscale.

The atmosphere is not an infinite simply-connected demain, and this, combined with its rotation, must force a state of non-homogeneity, even in the horizontal, on the largest scale. Other limitations of the present treatmeants will occur to the

meteorological reader, but we would prefer to close on a hopeful note in remarking on the progress made towards our needs by the extension to anisotropy and to a turbulent field assumed to exist without mean motion.

Acknowledgements. The authors are thankful to Dr. Nelson de Jesus Parada, Director, and Dr. Antonio Divino Moura, chief to the Department of Meteorology, Instituto de Pesquisas Espaciais, São José dos Campos, São Paulo, Brazil, for their encouragement. They would like to acknowledge the assistence of Mr. José Carlos Moreira in the Landsat imagery analysis. Thanks are due to Dr. Renato Herz for reading the manuscript, Mr. Carlos Roberto dos Santos and his group members for drafting the figures and Miss Célia Regina Rosa for typing the manuscript. This work was partially supported by the Financiadora de Estudos e Projetos (FINEP) under contract B/54/81/042/00/00.

Griggs, M., Determination of aerosol constant of the atmosphere. In symposium on significant results obtained from the earth resources technology satellite, NASA, Goddard Space Flight Center, Greenbelt, MD., 1973.

Holland, J. Z., A meteorological survey of the OaK Ridge area: Final report covering the period 1948-1952. USAEC Rept. ORO-99, Weather Bureau, OaK Ridge, Tennessee, 1953.

Hanna, S. R., A method of estimating vertical eddy transport in the planetary Boundary layer using characteristics of the vertical velocity spectrum, J. Atmos. Sci., 23, 1026-1033, 1968.

Hanna, S. R., Lagrangian and Eulerian Time-Scale relations in the daytime boundary layer, J. Appl. Meteorol., 20, 242-249, 1981.

Heisenberg, W., Zur statistischen theorie der turbulenz, Z. Physik, 124, 628-657, 1948a.

Heisenberg, W., On the theory of statistical and isotropic turbulence, Proc. Roy. Soc., London, A, 195, 402-406, 1948b.

Högström, U., An experimental study of atmospheric diffusion, Tellus, 16, 205-251, 1964.

Inoue, E., On the turbulent structure of airflow within crop canopies, J. Meteor. Soc. Japan, 41, 317-325, 1963.

Insitituto Nacional de Meteorologia, Meteorological data of 1968 to 1978 from the station, Fabrica Nacional de Alkalis, Cabo Frio, Instituto Nacional de Meteorologia, Brazil, 1968-1978.

Kellogg, W. W., Diffusion of smoke in the stratosphere, J. Meteorol., 13, 241-250, 1956.

Koprov, V. M., and L. R. Tsvang, Characteristics of very small-scale turbulence in a stratified boundary layer, Izv. Atmos. Ocean. Plys., 2, 705-709, 1966.

Kukharets, V. P., and L. R. Tsvang, The turbulent energy dissipation rate in an unstably stratified atmospheric boundary layer, Izv. Atmos. Ocean. Phys., 13, 419-424, 1977.

Lavoie, R. L., A mesoscale numerical model of lake effect storms, J. Atmos. Sci., 29, 1025-1040, 1972.

Lenschow, D. H., Two examples of planetary boundary layer modification over the Great Lakes, J. Atmos. Sci., 30, 568-581, 1973.

25 & 26

PRECEDING PAGE BLANK NOT FILMED

Lettau, H. H., Dissipation of energy by turbulence, J. Meteorol., 18, 125-126, 1961.

Lilly, D. K., D. E. Waco and S. I. Adelfang, Stratospheric mixing estimated from high-altitude turbulence measurements, J. Appl. Meteorol., 13, 488-493, 1974.

Lyons, W. A., and S. R. Pease, Detection of particulate air pollution plumes from major-point sources using ERTS-imagery, Bull. Amer. Meteor. Soc., 54, 1163-1170, 1973.

Lyons, W. A., Satellite detection of air pollutants. In Remote Sensing Energy-Related Studies (edited by T. N. Vaziroglu), pp. 263-290, John Wiley, New York, 1975a.

Lyons, W. A., Turbulent diffusion and pollutant transport in shoreline environment. In Lectures on air pollution and environmental impact analysis, Amer. Meteor. Soc., Boston, Mass., U.S.A., 136-208, 1975b.

McLellan, A., Satellite remote sensing of large scale local atmospheric pollution. In Proc. Int. Clear Air Congr. 1380-1388, Air Pollution Control Association, Pittsburgh, PA., 1971.

Mekler, Y., H. Quenzel, G. Ohring and I. Marcels, Relative atmospheric aerosol content from ERTS observations, J. Geophys. Res., 82, 967-970, 1977.

Miyake, M., M. Donelan and Y. Mitsuta, Airbone measurements of turbulent flux, J. Geophys. Res., 75, 4506-4518, 1970.

Nicolli, D., Altura da camada de inversão térmica e potencial de poluição do ar, Relatório DR/GAL(MTL)-001-77, Comissão Nacional de Energia Nuclear, Brazil, 38 pp, (in portuguese), 1977.

Pasquill, F., The estimate of the dispersion of windborne material, Meteor. Mag., 90, 33-46, 1961.

Pasquill, F., Atmospheric diffusion, D. Van Nostrand Company Ltd., New York, 1962.

Pasquill, F., Atmospheric dispersion of pollution, Q. J. R. Meteorol. Soc., 97, 369-395, 1971.

Phillips, D. W., Modification of surface air over Lake Ontario in winter, Mon. Wea. Rev., 100, 662-670, 1972.

Pond, S., G. T. Phelps and J. E. Paquin, Measurements of the turbulent fluxes of momentum, moisture and sensible heat over the ocean, J. Atmos. Sci., 28, 901-917, 1971.

Pond, S., and K. Bryan, Numerical models of the ocean circulation, Rev. Geophys. Space Phys., 14, 243-263, 1976.

Prophet, D. T., Survey of the available information pertaining to the transport and diffusion of airbone material over ocean and shoreline compleses, Tech. Rep. nº 89, Aerosol Lab., Stanford University, 53 pp., 1961.

Randerson, D., A study of air pollution sources as viewed by earth satellite, J. Air Pollution Control. Assoc., 18, 249-253, 1968.

Randerson, D., J. G. Garcia and V. S. Whitehead, Photogrammetric and Photometric investigation of a smoke plume viewed from space, J. Appl. Meteorol., 10, 1122-1131, 1971.

Rayment, R., An observational study of the vertical profile of the high frequency fluctuations of the wind in the atmospheric boundary Layer, Bound.-Layer Meteorol., 3, 284-300, 1972.

Raynor, G. S., P. Michael, R. M. Brown and S. SethuRaman, Studies of atmospheric diffusion from a nearshore ocean site, J. Appl. Meteorol., 14, 1080-1094, 1975.

Raynor, G. S., R. M. Brown and S. SethuRaman, A comparison of diffusion from a small island and a undisturbed ocean site, J. Appl. Meteorol., 17, 129-139, 1978.

Readings, C. T., Some aspects of the Cardington research programme, Q. J. Roy. Meteorol. Soc., 99, 764-766, 1973.

Record, F. A., and H. E. Cramer, Turbulent energy dissipation rates and exchange processes above a non-homogeneous surface, Q. J. R. Meteorol. Soc., 92, 519-532, 1966.

Remsberg, E. E., Diffusion in the lower stratosphere as determined from lider measurements of volcanic aerosol dispersion, J. Atmos. Sci., 37, 2105-2112, 1980.

Richardson, L. F., I. Some measurements of atmospheric turbulence, Phil. Trans. Roy. Soc. London, A, 221, 1-28, 1920.

Richardson, L. F., Atmospheric diffusion shown on a distance--neighbour graph, Proc. Roy. Soc. London, A, 110, 709-737, 1926.

Roll, H. U., Physics of the Marine Atmosphere, Academic Press, New York, 344-348, 1965.

Roberts, O. F. T., The theoretical scattering of smoke in a turbulent atmosphere, Proc. Roy. Soc. London, A, 104, 640-654, 1923.

Saffman, P. G., The effect of wind shear on horizontal spread from an instantaneous ground source, Q. J. R. Meteorol. Soc., 88, 382-393, 1962.

Silva, P. de C. M., Upwelling and its biological effects in Southern Brazil. In Fertility of the Sea-2 (edited by J. D. Costlow Jr.), Gordon and Breack Science Pub., New York, 469-474, 1971.

Slade, D. H., Atmospheric dispersion over Chesapeake Bay, Mon. Wea. Rev., 90, 217-224, 1962.

Smith, F. B., The role of wind shear in horizontal diffusion of ambient particles, Q. J. R. Meteorol. Soc., 91, 318-329, 1965.

Sutton, O. G., A theory of eddy diffusion in the atmosphere, Proc. Roy. Soc. London, A, 135, 143-165, 1932.

Sutton, O. G., Convection in the atmosphere near the ground, Q. J. R. Meteorol. Soc., 74, 13-30, 1948.

Sutton, O. G., Micrometeorology, McGraw-Hill Book Company, New York, 1953.

Takeuchi, K., and S. Ito, Estimation of the diffusion coefficient of thermal pollution, Adv. Geophys., 16A., Academic Press, New York, 384-390, 1974.

Taylor, G. I., Diffusion by continuous moments, Proc. London Math. Soc., 2, 196-211, 1921.

Taylor, R. J., Aircraft measurements of dissipation of turbulent kinetic energy, Q. J. R. Meteorol. Soc., 98, 658-661, 1972.

Tsuchiya, K., and T. T. Fujita, A satellite meteorological study of evaporation and cloud formation over the western Pacific under the influence of the winter monsoon, J. Meteorol. Soc. Japan, 45, 232-250, 1967.

Tyldesley, I. B., and C. E. Wallington, The effect of wind shear and vertical diffusion on horizontal disperson, Q. J. R. Meteorol. Soc. 91, 158-174, 1965.

Van der Hoven, I., Atmospheric transport and diffusion at coastal sites, Nucl. Safety, 8, 409-499, 1967.

Vaughan, E. M., The prediction of atmospheric diffusion by using an eddy diffusivity based on vertical transfer of heat, J. Meteorol., 18, 43-49, 1961.

Vinnichenko, N. K., and J. A. Dutton, Empirical studies of atmospheric structure and spectra in the free atmosphere, Radio Science, 4, 1115-1126, 1969.

Volkov, Yu. A., V. P. Kukharets, and L. R. Tsvang, Turbulence in the atmospheric boundary layer above steppe and sea surface, Izv. Atmos. Ocean. Phys., 4, 591-599, 1968.

Volkovitskaya, Z. I., and V. N. Ivanov, Turbulent energy dissipation of the atmospheric boundary layer, Izv. Atmos. Ocean. Phys., 6, 435-444, 1970.

Wamser, C., and H. Muller, On the spectral scale of wind fluctuations within and above the surface layer, Q. J. R. Meteorol. Soc., 103, 721-730, 1977.

Warner, J., The structure and intensity of turbulence in air over the sea, Q. J. R. Meteorol. Soc., 98, 175-186, 1972.

Weinstock, J., Vertical turbulent diffusion in a stably stratified fluid, J. Atmos. Sci., 35, 1022-1027, 1978.

Whitehead, V. S., I. D. Browne and J. G. Garcin, Cloud height contouring from Apollo 6 photography, Bull. Amer. Meteor. Soc., 50, 522-528, 1969.

World Meteorological Organization, Climatic Atlas of South America-I, WMO, Unesco, Catographia 1975, Hungary, 1975.

Yamamoto, S., M. Gamo and O. Yokoyama, Airborne measurements of turbulent heat flux, J. Meteor. Soc. Japan, 55, 533-545, 1977.

List of tables

List of figures

Fig. 1. Map of a portion of the Brazilian coastal area showing Cabo Frio region, Fábrica National de Alcalis and Airport of Galeão. Ocean depth contour lines are in 50 m intervals.

Fig. 2. Evaluation of σ_y from the Landsat image of 1144 GMT 8 December 1975 for the Cabo Frio region.

Fig. 3. An April 18, 1975 Landsat image at 1157 GMT of smoke plume of the Cabo Frio region drifting NE wards across the Atlantic Ocean. It has an initial portion of 50 km long, and associated with a horizontal wind speed, $u = 4.8$ m s^{-1}, and a vertical temperature gradient, $\frac{\partial \theta}{\partial z} = -7.2$ K km^{-1}. There is a discontinuity of the plume approximately at about 15 km distance from the source. Image photographically enhanced from original 35 mm slide.

Fig. 4. As in Fig. 3 except for 1144 GMT 8 December 1975. The plume has an initial portion of 40 km long, and is associated with $u = 4.6$ m s^{-1} and $\frac{\partial \theta}{\partial z} = -7.0$ K km^{-1}. There were no clouds present in this view, only turbid and hazy conditions due to upwelling in this period.

Fig. 5. As in Fig. 3 except for 1139 GMT 18 February 1976. The plume has an initial portion of 40 km long, and is associated with $u = 1.6$ m s^{-1} and $\frac{\partial \theta}{\partial z} = -1.6$ K km^{-1}. It has a concave nature approximately between 10 to 18 km distances from the source. Cumulus clouds are visible on left side of photo.

Fig. 6. As in Fig. 3 except for 1138 GMT 7 March 1976. The air was s slightly unstable that the plume could be seen extending for 120 km with $u = 6.4$ m s^{-1} and $\frac{\partial \theta}{\partial z} = -6.1$ K km^{-1}. It is a well defined plume with marked boundaries.

Fig. 7. As in Fig. 3 except for 1130 GMT 23 June 1976. The air was so stable that the plume could be seen extending for 130 km with $u = 4.1$ m s^{-1} and $\frac{\partial\theta}{\partial z} = 5.6$ K km^{-1}. But, over water fetch the air temperature was slightly colder than the ocean surface temperature. The formation of cumulus clud streets are visible over the ocean in right side of photo.

Fig. 8. As in Fig. 3 except for 1150 GMT 3 February 1977. The plume is not a well defined one. It is exhibiting mixing in the shallow turbulent layer above the ocean. It has an initial portion of 40 km long, and associated with high value of $u = 10.7$ m s^{-1} and $\frac{\partial\theta}{\partial z} = -7.7$ K km^{-1}. Image quality is severely degraded by rephotography.

Fig. 9. As in Fig. 3 except for 1153 GMT 11 March 1977. The plume is not a well defined one. In this case the water temperature is slightly colder than air temperature. It has an initial portion of 100 km long, and is associated with $u = 8.0$ m s^{-1} and $\frac{\partial\theta}{\partial z} = 0.6$ K km^{-1}. It can be seen that the conditions of the atmosphere were hazy and granular.

Fig. 10. As in Fig. 3 except for 1145 GMT 22 May 1977. The plume has more than 20 km long in length. It is drifting SW wards with $u = 4.0$ m s^{-1} and $\frac{\partial\theta}{\partial z} = 4.7$ K km^{-1}. Water temperature is slightly greater than air temperature, but the radiosonde ascent showed the surface and higher level inversions. The plume is exhibiting mixing and undefined boundary contours.

Fig. 11. As in Fig. 3 except for 1144 GMT 9 June 1977. The plume has more than 30 km long in length. It is drifting SW and W wards with $u = 3.3$ m s^{-1} and $\frac{\partial\theta}{\partial z} = -6.0$ K km^{-1}. The ocean surface temperature is greater than air temperature. It is exhibiting undefined contour pattern in a turbid and hazy atmosphere.

Fig. 12. As in Fig. 3 except for 1136 GMT 31 October 1977. The air was so stable that the plume could be seen extending for 80 km with $u = 5.0$ m s^{-1} and $\frac{\partial\theta}{\partial z} = 7.0$ K km^{-1}. Image quality is degraded by rephotography.

Fig. 13. As in Fig. 3 except for 1205 GMT 1 July 1978. The air was so stable that the plume could be seen extending for 130 km with $u = 4.6$ m s^{-1} and $\frac{\partial\theta}{\partial z} = 2.7$ K km^{-1}. A strong clockwise surface water current is visible on right side of the island.

Fig. 14. Maximum plume width Y_m (from Table 3) in relation to wind speed at a stack height of 76 m for quasi-neutral and stable conditions of stability.

Fig. 15. Values of σ_y^2 as a function of downwind distance (x) in quasi-neutral and stable conditions.

Fig. 16. As in Fig. 15 except for stable conditions.

Fig. 17. (a) Variation of mean lateral diffusion coefficient K_y (from Table 2) with wind speed at a stack height of 76 m in quasi-neutral conditions. (b) As in (a) except for mean vertical diffusion coefficient K_z (from Table 4) in stable conditions.

TABLE 1. Reference number of Landsat image cases (n) and various meteorological parameters.

n	Date	Time in hours		C	Wind Speed $m\ s^{-1}$		DDD	Temperature °C		$\frac{\partial\theta}{\partial z}$	Inversion height m		RI
		G.M.T.	Local		10 m	76 m		T_s	T_h	K/100 m	Base	Top	
1	18-04-75	1157	0857	20	1.0	4.8	N	25.0	24.4	-0.72	1600	2000	-0.071
2	08-12-75	1144	0844	40	(-)	4.6	NE	25.0	24.5	-0.70	-	-	-0.065
3	18-02-76	1139	0839	50	5.8	1.6	NNE	27.0	26.8	-0.16	-	-	-0.013
4	07-03-76	1138	0838	10	(-)	6.4	NE	26.0	25.5	-0.61	-	-	-0.028
5	23-06-76	1130	0830	0	8.3	4.1	NNE	23.0	23.5	0.56	1300	1500	0.046
6	03-02-77	1150	0850	10	7.1	10.7	NE	26.0	25.4	-0.77	-	-	-0.085
7	11-03-77	1153	0853	10	4.1	8.0	NE	28.0	28.2	0.06	Surface	400	0.006
8	22-05-77	1145	0845	40	1.1	4.0	W	21.0	21.5	0.47	Surface 1800	900 2500	0.081
9	09-06-77	1144	0844	0	(-)	3.3	W	22.0	21.5	-0.60	-	-	-0.106
10	31-10-77	1136	0836	20	10.0	5.0	NNE	26.0	26.6	0.70	Surface	400	0.040
11	01-07-78	1205	0905	0	2.5	4.6	N	23.0	23.2	0.27	Surface	500	0.088

C = cloud cover in percent; DDD = prominent wind direction; T_s = screen temperature; T_h = 76 m stack height temperature; $\partial\theta/\partial z$ = potential temperature gradient below 80 m; RI = Richardson gradient number. (-) means missing data.

The wind speed at 76 m stack height level, T_h and $\partial\theta/\partial z$, are obtained from radiossonde ascents at the international airport of Galeão. The stability parameter RI is calculated using mean value of T_s and T_h, and the wind shear between 10 and 76 m. In the case of missing wind data at 10 m level, the wind shear is obtained after dividing the 76 m-level wind speed by 76 m.

TABLE 2. Estimated lateral standard deviation, σ_y (m), and lateral eddy diffusivity coefficient, K_y ($m^2\ s^{-1}$), from Landsat images.

n	RI	$\bar{u}$ m s^{-1}			Distance from source in km 1	5	10	15	20	Mean
1	- 0.071	4.8	σ_y		100	260	520	-	-	293.33
			K_y		10.56	116.54	-	-		63.55
2	- 0.065	4.6	σ_y		97	329	620	930	1220	639.20
			K_y		56.83	127.03	221.03	286.81		172.93
3	- 0.013	1.6	σ_y		80	160	341	601	862	408.80
			K_y		3.84	14.51	39.19	61.10		29.66
4	- 0.028	6.4	σ_y		80	220	421	621	782	424.80
			K_y		33.6	82.46	133.38	246.81		124.06
5	0.046	4.1	σ_y		72	136	218	309	454	237.80
			K_y		6.82	11.90	19.66	45.36		20.94
6	- 0.085	10.7	σ_y		70	270	600	-	-	313.33
			K_y		90.95	307.20				199.07
7	0.006	8.0	σ_y		116	552	800	988	1162	723.60
			K_y		291.25	268.24	268.92	299.28		281.92
8	0.081	4.0	σ_y		80	401	-	-	-	240.50
			K_y		61.76	-	-	-		61.76
9	- 0.106	3.3	σ_y		116	543	601	698	891	569.80
			K_y		116.08	21.90	41.58	101.20		70.19
10	0.040	5.0	σ_y		79	224	469	612	734	423.60
			K_y		21.97	84.89	77.29	82.11		66.56
11	0.088	4.6	σ_y		84	169	258	328	412	250.20
			K_y		12.37	17.48	18.87	28.59		19.33

$\bar{u}$ = Mean wind speed at 76 m stack height level. K_y is calculated from Eq. (2).

TABLE 3. Lateral eddy diffusivity coefficient (K_y) values derived from smoke plumes of the Landsat imagery

n	RI	$\bar{u}$ m s^{-1}	X_t km	X_m km	Y_m m	$(K_y)_4$ m^2 s^{-1}	$(K_y)_5$ m^2 s^{-1}	Mean $(K_y)_2$ m^2 s^{-1}	$\frac{(K_y)_5}{(K_y)_4}$	$\frac{(K_y)_2}{(K_y)_4}$
1	- 0.071	4.8	50	5	1118.9	83.73	599.96	63.55	7.17	0.76
2	- 0.065	4.6	40	5	1414.7	160.60	1634.74	172.93	10.18	1.08
3	- 0.013	1.6	40	10	1466.3	60.01	172.00	29.66	2.87	0.49
4	- 0.028	6.4	120	10	1810.3	121.96	1048.70	124.06	8.60	1.02
5	0.046	4.1	130	10	937.4	19.34	180.14	20.94	9.31	1.08
6	- 0.085	10.7	40	5	1161.0	251.60	1442.28	199.07	5.73	0.79
7	0.006	8.0	100	5	2373.6	314.50	4507.18	281.92	14.33	0.90
8	0.081	4.0	20	1	344.0	16.51	236.67	61.76	14.33	3.74
9	- 0.106	3.3	30	5	2334.9	418.45	1799.08	70.19	4.30	0.17
10	0.040	5.0	80	5	958.9	40.10	459.74	66.56	11.46	1.66
11	0.088	4.6	130	5	726.7	13.04	242.92	19.33	18.63	1.48

X_t is total plume length. X_m is the distance downwind from the source at which the maximum plume width Y_m occurs (see Eq. (8), $Y_m = 2\ Y_0 = 4.3\ \sigma_y$). Mean $(K_y)_2$ is from Table 2. $(K_y)_4$ and $(K_y)_5$ are derived from Eqs. (4) and (5), respectively.

TABLE 4. Estimation of the rate of kinetic energy dissipation (ε) and vertical eddy diffusivity coefficient (K_Z) from smoke plumes of the Landsat imagery.

n	RI	$\overline{T}$ K	$\frac{\partial\theta}{\partial z}$ K/100 m	N^2 s^{-2} x 10^{-4}	Mean σ_y m	Mean K_y $m^2\ s^{-1}$	Mean ε $m^2\ s^{-3}$ x 10^{-5}	Mean K_z $m^2\ s^{-1}$
1	- 0.071	297.7	- 0.72	-	293.33	63.55	3.469	-
2	- 0.065	297.8	- 0.70	-	639.20	172.93	3.100	-
3	- 0.013	299.9	- 0.16	-	408.80	29.66	0.094	-
4	- 0.028	298.8	- 0.61	-	424.80	124.06	5.899	-
5	0.046	296.3	0.56	1.852	237.80	20.94	0.287	0.013
6	- 0.085	298.7	- 0.77	-	313.33	199.07	80.190	-
7	0.006	301.1	0.06	0.195	723.60	281.91	8.227	3.417
8	0.081	294.3	0.47	1.565	240.50	61.76	7.045	0.365
9	- 0.106	294.8	- 0.60	-	596.80	70.19	0.328	-
10	0.040	299.3	0.70	2.292	423.60	66.56	0.917	0.032
11	0.088	296.1	0.27	0.894	250.20	19.33	0.184	0.017

N = The Brunt Väisälä frequency. $\overline{T}$ is equal to $(T_S + T_h)/2$ from Table 1. Mean values of σ_y and K_y are from Table 2.

TABLE 5. Summary of ε, K_y and K_z from the literature.

Source	Location	Height m	ε $m^2\ s^{-3}$ x 10^{-5}	K_y $m^2\ s^{-1}$	K_z $m^2\ s^{-1}$
1. Sutton (1948)	Land areas	Lowest 100	-	-	50.000
2. Sutton (1953)	Land areas	Ground level	-	1.60	0.500
3. Ball (1961)	Land site, Australia	12-153	0.10-10.00	-	-
4. Lettau (1961)	Various sites	0.01-4x10^4	10^{7}-10^{-2}	-	-
5. Vaughan(1961)	O'Neill, Nebraska	1	-	-	0.006-0.328
6. Pasquill (1962)	Land areas	2	-	-	0.130-0.560
7. Inoue (1963)	Paddy Surface, Japan	0.4-0.85	111-14.80	-	-
8. Roll (1965)	Over water	Surface-75	-	-	0.050-3.500
9. Koprov and Tsvang (1966)	Over steppe Area, USSR	50-500	100-0.40	-	-
"	"	8-270	130-4	-	-
10. Record and Cramer (1966)	Round Hill, USA	16-40	4580-80	-	-
11. Hanna (1968)	Round Hill, Cedar Hill, USA	15-229	12500-12.50	-	0.100-12.00
12. Volkov et al. (1968)	Over steppe area and sea surface	20-750	1-0.02	-	-
13. Vinnichenko and Dutton (1969)	-	1x10^3-2x10^4	4800-21	-	-
14. Clarke (1970)	Kerang and Hay, Australia	30-600	610-13	-	-
15. Miyake et al. (1970)	BOMEX array	sea Surface-18.3	300	-	-
16. Volkovitskaya and Ivanov (1970)	Land area, USSR	8-180	5.50-0.02	-	-
17. Pasquill(1971)	Land area	10-100	-	-	0.120-30.00
18. Pond et al. (1971	Ocean area near San Diego, California	8	918-234	-	-
19. Randerson et al. (1971)	Arizona, USA	-	-	44.60-85.90	15.00-30.90

(Continue)

Table 5. (continued)

Source	Location	Height m	ϵ $m^2\ s^{-3}$ x 10^{-5}	Ky $m^2\ s^{-1}$	Ky $m^2\ s^{-1}$
20. Garrett (1972)	Lough Neagh, Northern Ireland	Water surface 1-2	3200-130	-	-
21. Rayment (1972)	Cardington, England	40-600	320-6	-	-
22. Taylor (1972)	Land areas, Australia	10-1310	$14x10^3$-0.05	-	-
23. Warner (1972)	Cairns, Australia	Sea surface 10-600	700-20	-	-
24. Readings (1973)	Cardington, England	30-900	800-5	-	-
25. Bowden et al. (1974)	Sea areas, Irish sea	-	0.01	0.01-1	10^{-5}-10^{-2}
26. Lilly et al. (1974)	Over various countries	$14x10^3$-$21x10^3$	168-65.27	-	0.009-0.064
27. Takeuchi and Ito (1974)	Sea surface	-	1.00-0.10	10-20	-
28. Lyons (1975b)	Over water	-	-	-	1.50-3.00
29. Gamo et al. (1976)	Kanto Plain, Japan	200-1500	760-1	-	-
30. Pond and Bryan (1976)	Ocean area	Surface-500 m depth	-	100	0.010
31. Bunker (1977)	East China sea, Pacific ocean	150-3300	110-2	-	-
32. Freeman (1977)	-	-	-	1.03-16.18	-
33. Kukharets and Tsvang (1977)	Over steppe area, USSR	50-2000	1000-1	-	-
34. Wamser and Muller (1977)	Hamburg, Germany	50-250	10^4-10	-	-
35. Yamamoto et al. (1977)	Kanto Plain, Japan	300-1500	165-0.10	-	-
	Kashima-land area, Japan	50-1500	114-0.10	-	-
	Kashima-sea surface, Japan	50-1500	23-0.10	-	-
	Shibushi-land area, Japan	100-1500	84-0.30	-	-
	Shibushi-sea area, Japan	100-150	108-0.10	-	-

(Continue)

Table 5.

Source	Location	Height m	ε $m^2\ s^{-3}$ x 10^{-5}	K_y $m^2\ s^{-1}$	K_z $m^2\ s^{-1}$
36. Gargett et al. (1979)	Sargasso sea	Surface-125 m depth	0.10-0.001	-	-
37. Fairal et al. (1980)	Panama City, USA	Surface-1000	10^4-1	-	-
38. Gregg and Sandford (1980)	Island of Bermuda	Surface-150 m depth	-	-	10^{-4}
39. Remsberg (1980)	Hawaii Virginia	$19x10^3$ $19x10^3$	- -	- -	0.015-0.150 0.056-0.420
40. Hanna (1981)	Boulder, USA	Surface-300	840-250	-	-

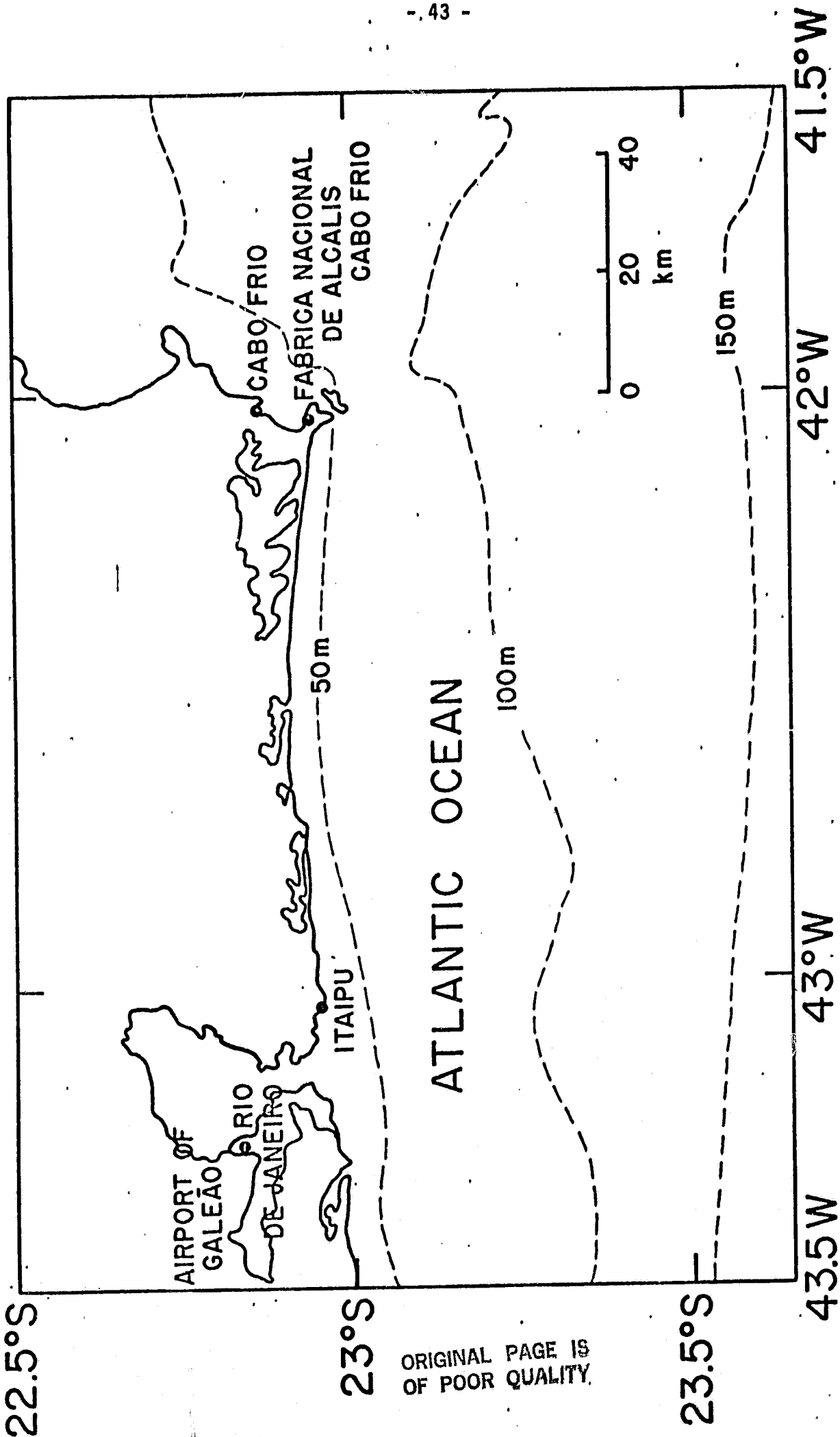

FIG. 1

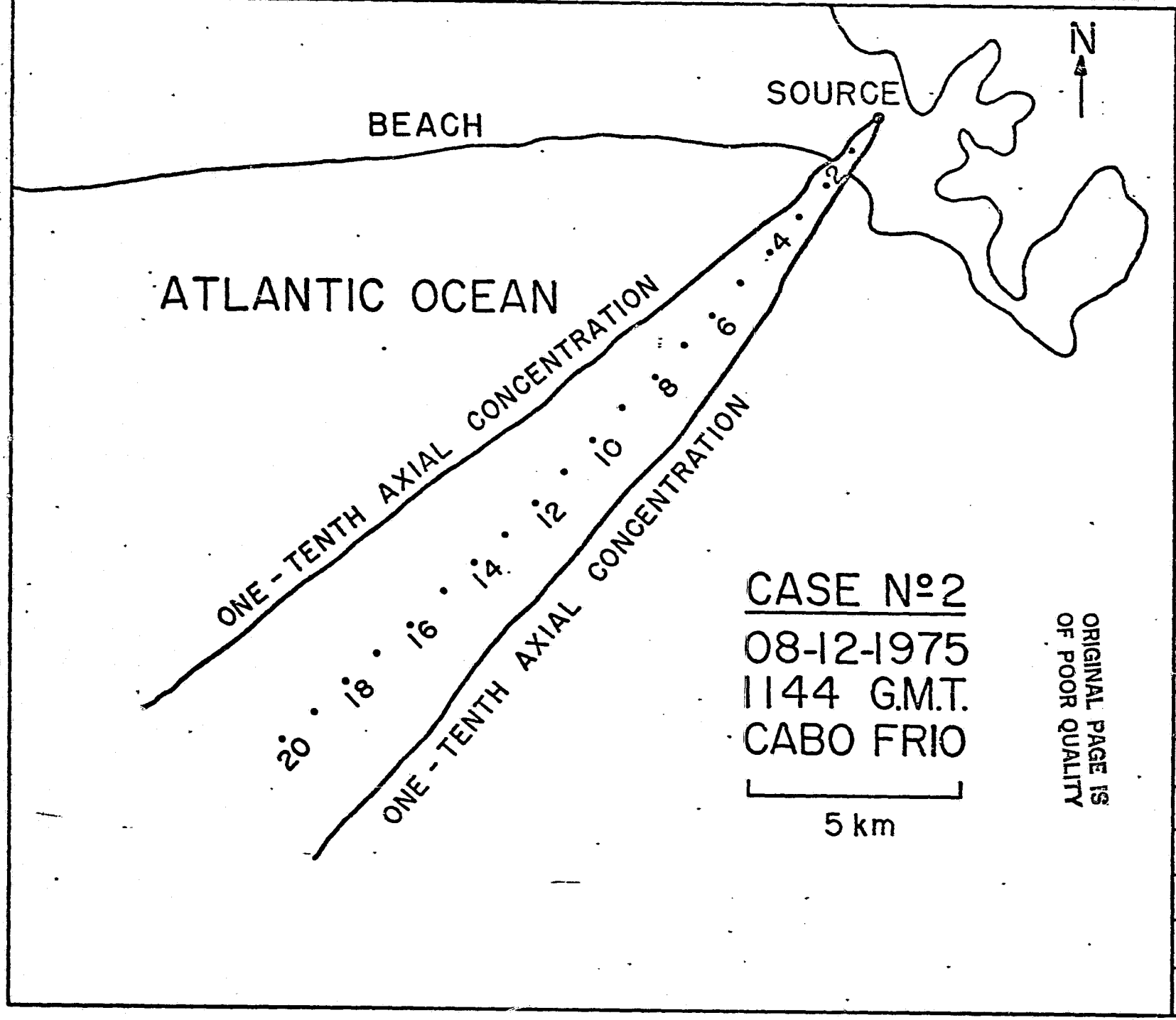

DIST. (km)	2Yo (m)	σ_y (m)
1	417	97
2	583	136
3	833	194
4	1166	271
5	1417	329
6	1667	387
7	2000	465
8	2250	523
9	2500	581
10	2666	620
11	2924	680
12	3182	740
13	3483	810
14	3741	870
15	4000	930
16	4214	980
17	4515	1050
18	4730	1100
19	4988	1160
20	5246	1220

FIG. 2

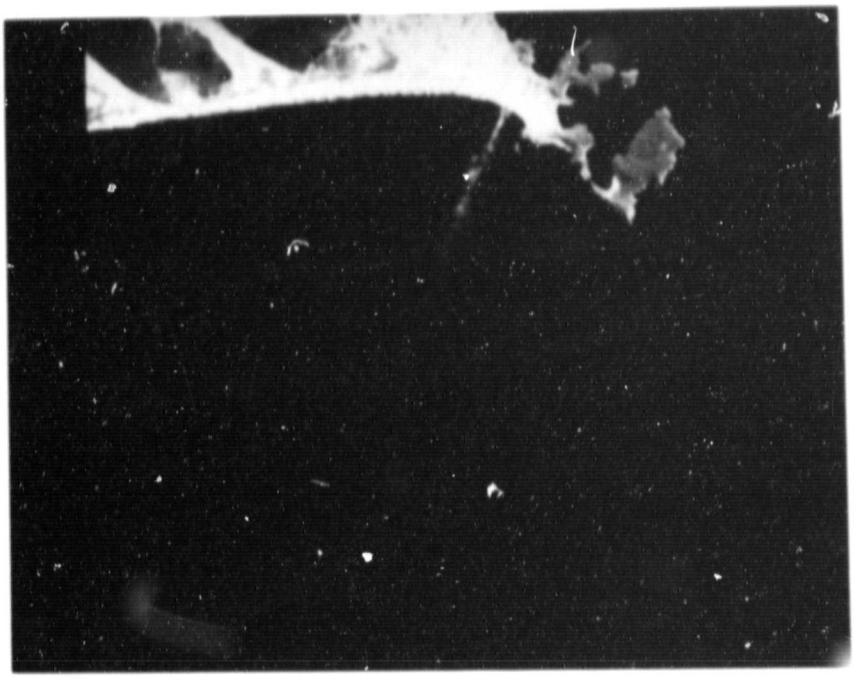

Fig. 3

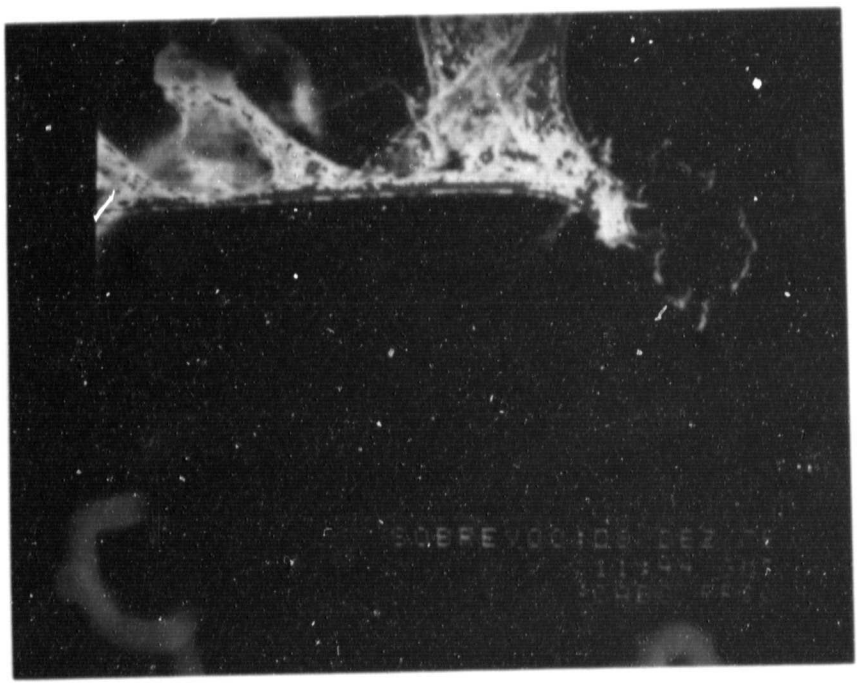

Fig. 4

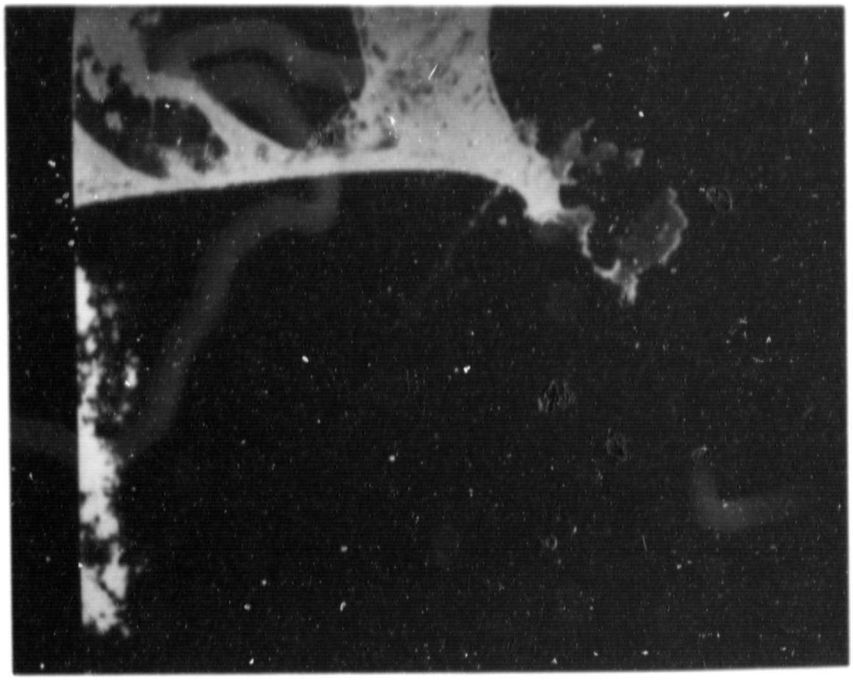

Fig. 5

Fig. 6

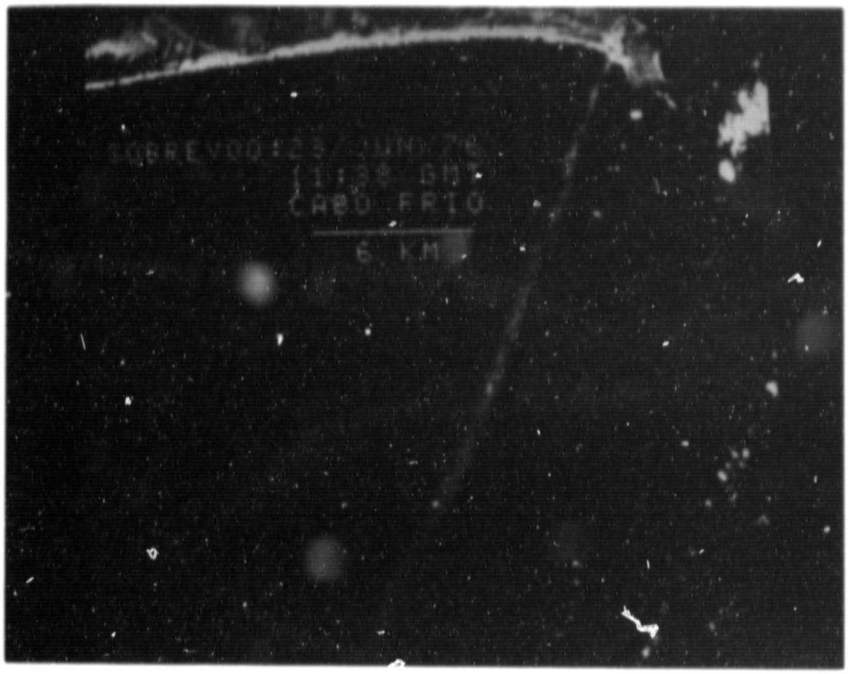

Fig. 7

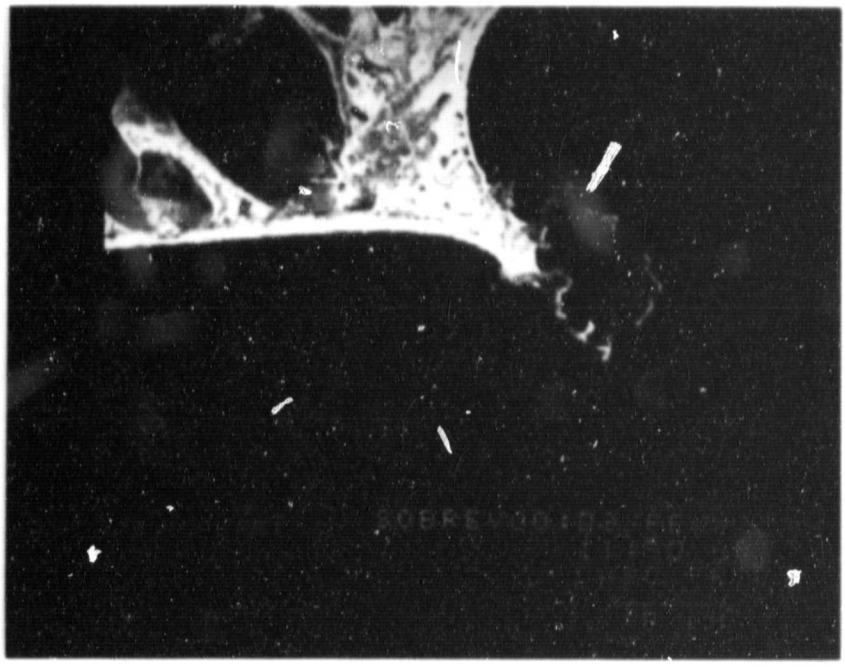

Fig. 8

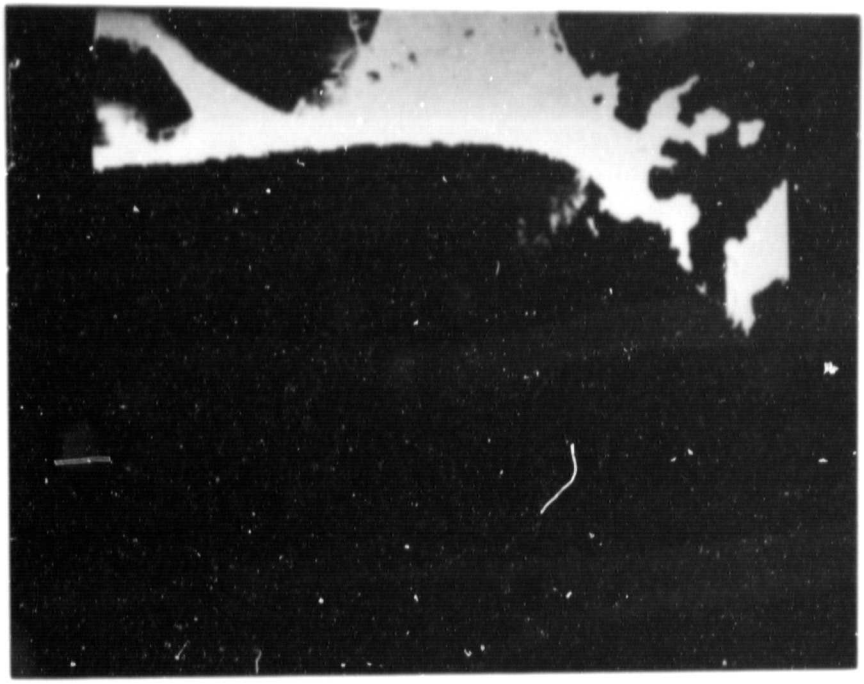

Fig. 9

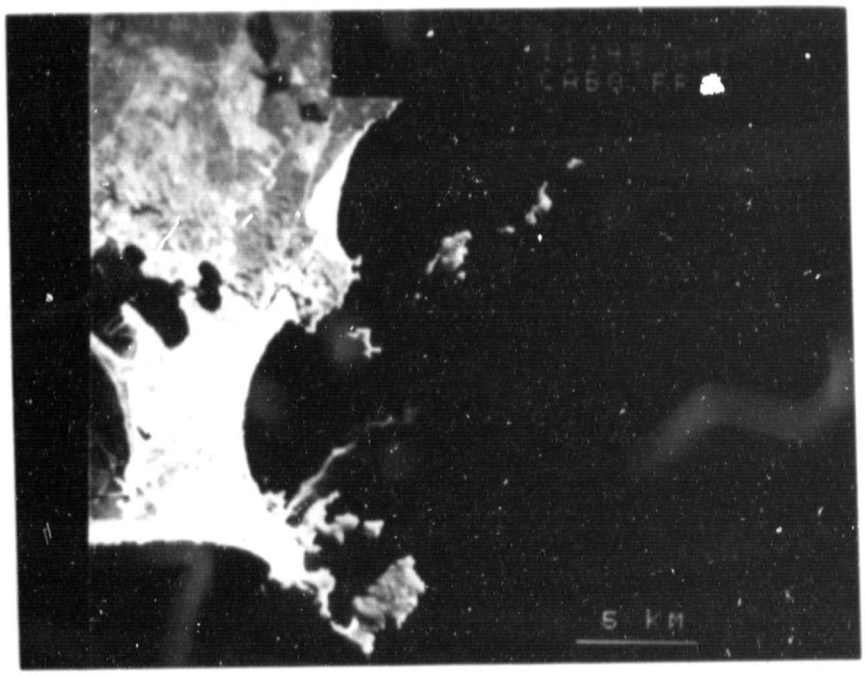

Fig. 10

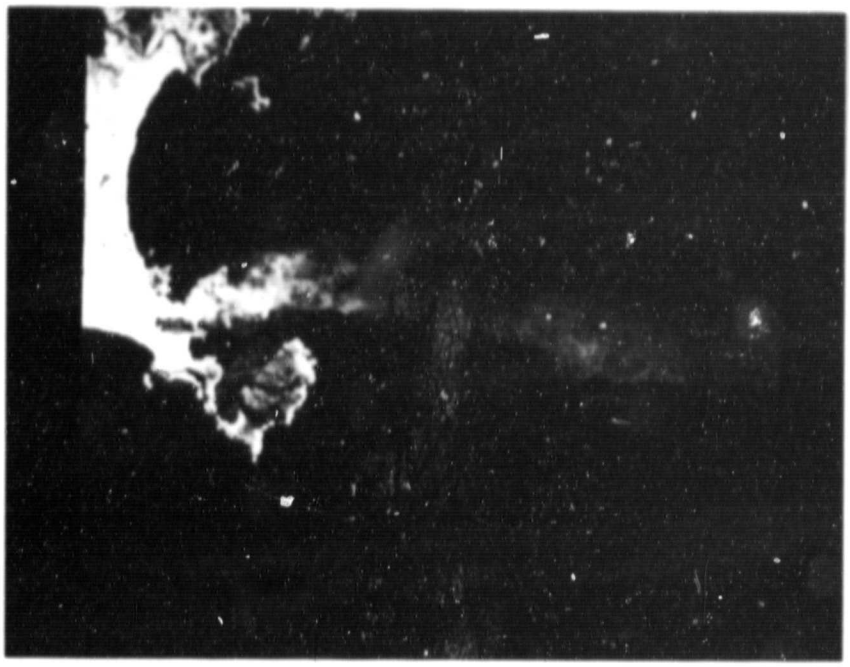

Fig. 11

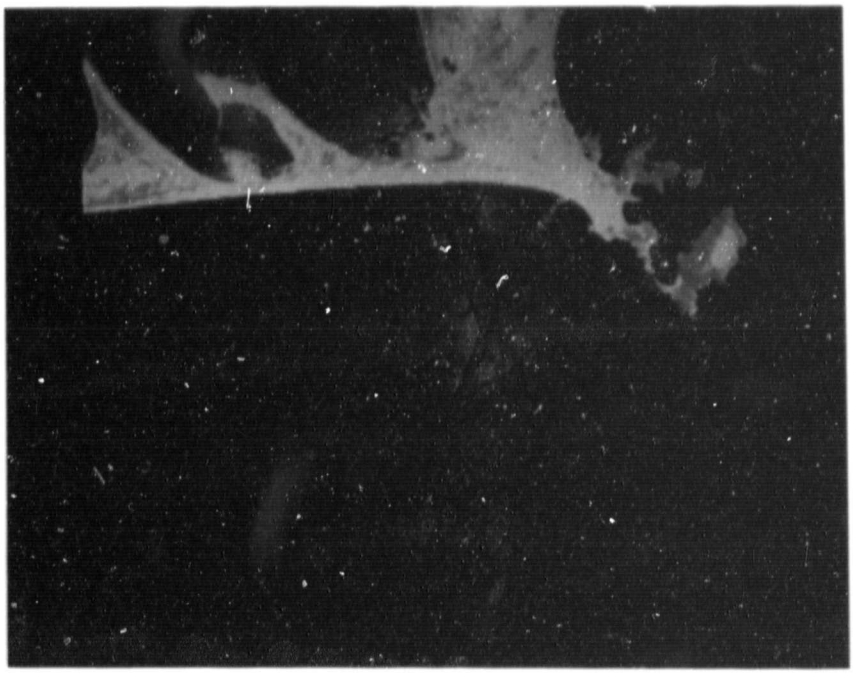

Fig. 12

Fig. 13

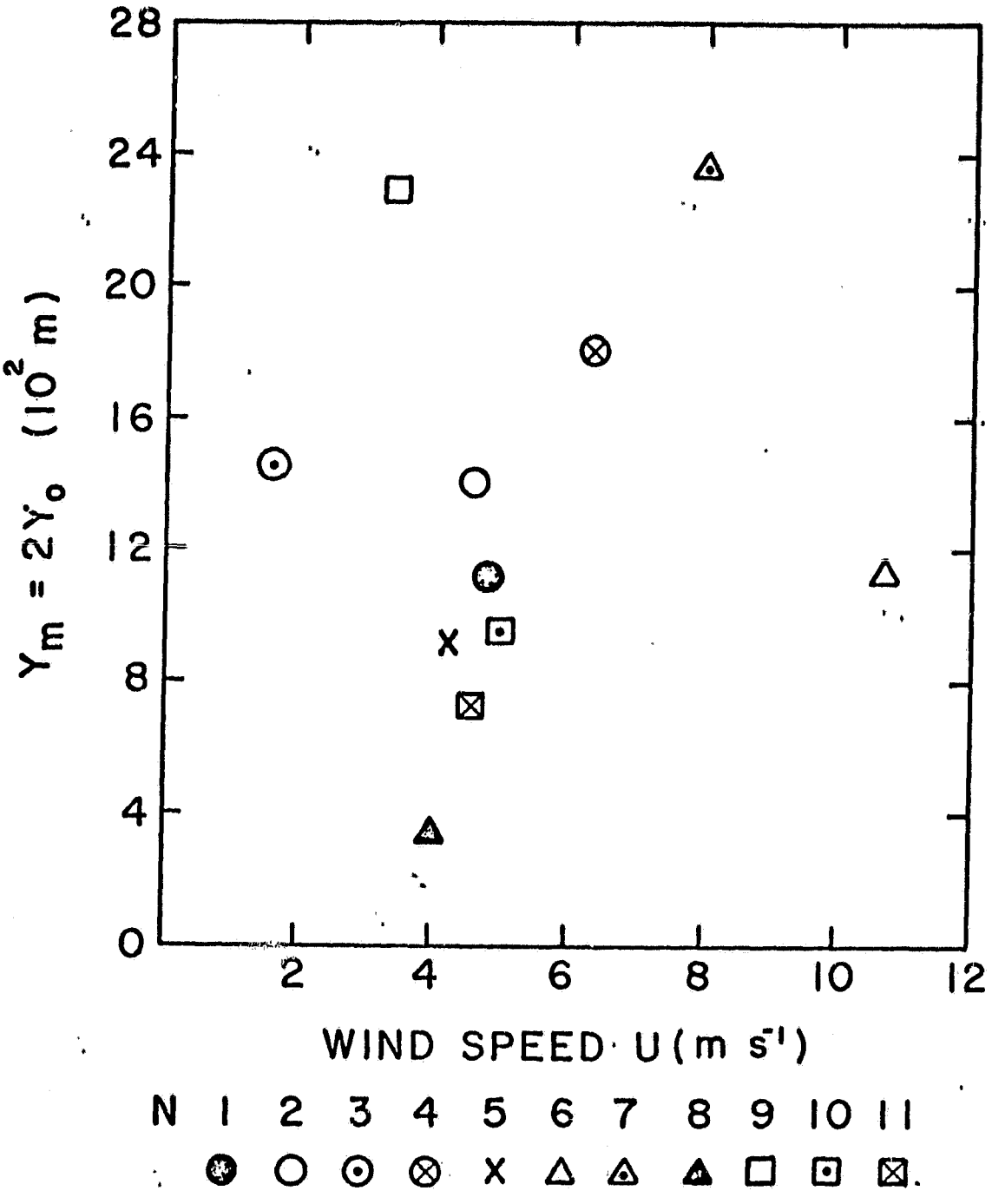

FIG. 14

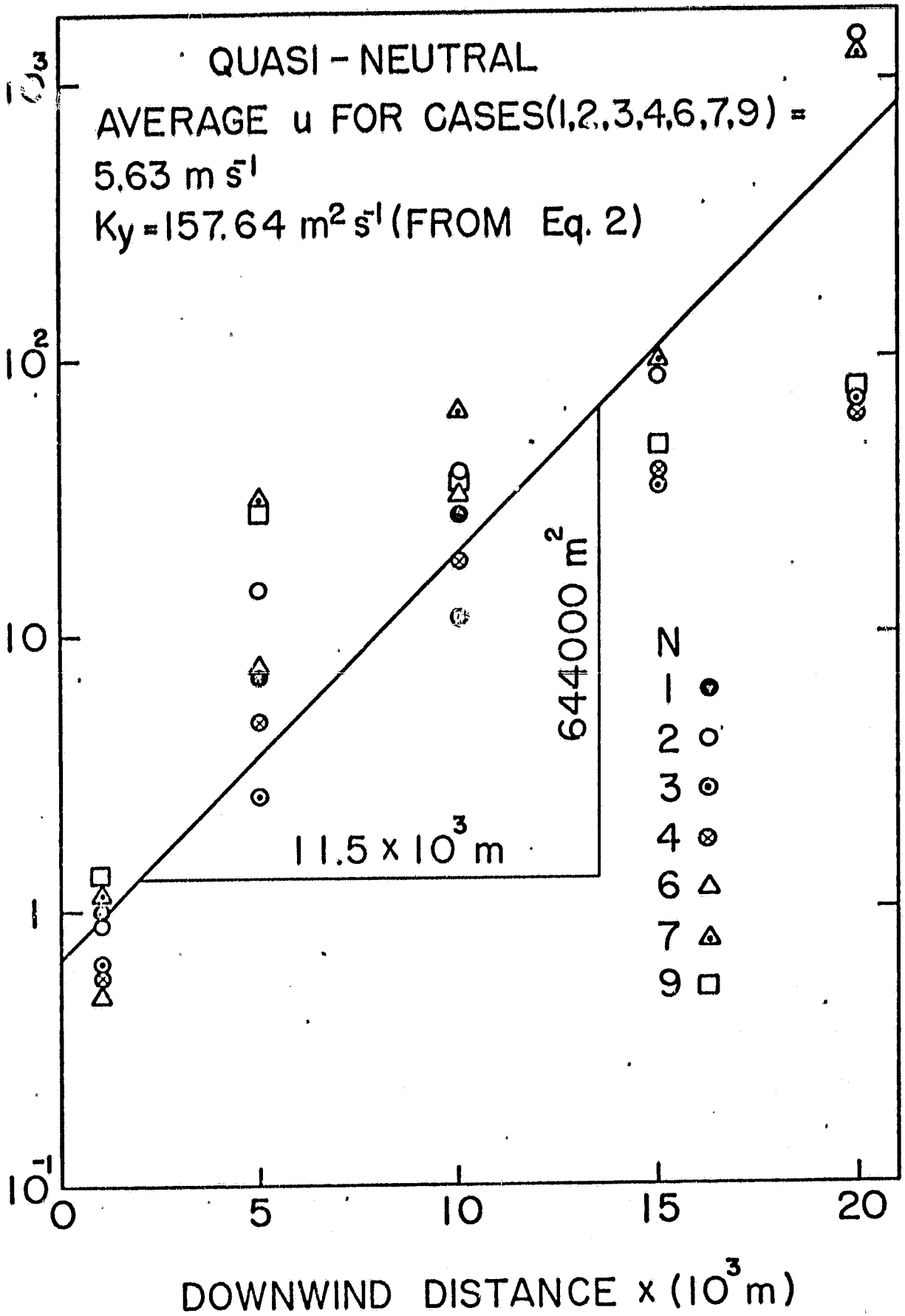

FIG. 15

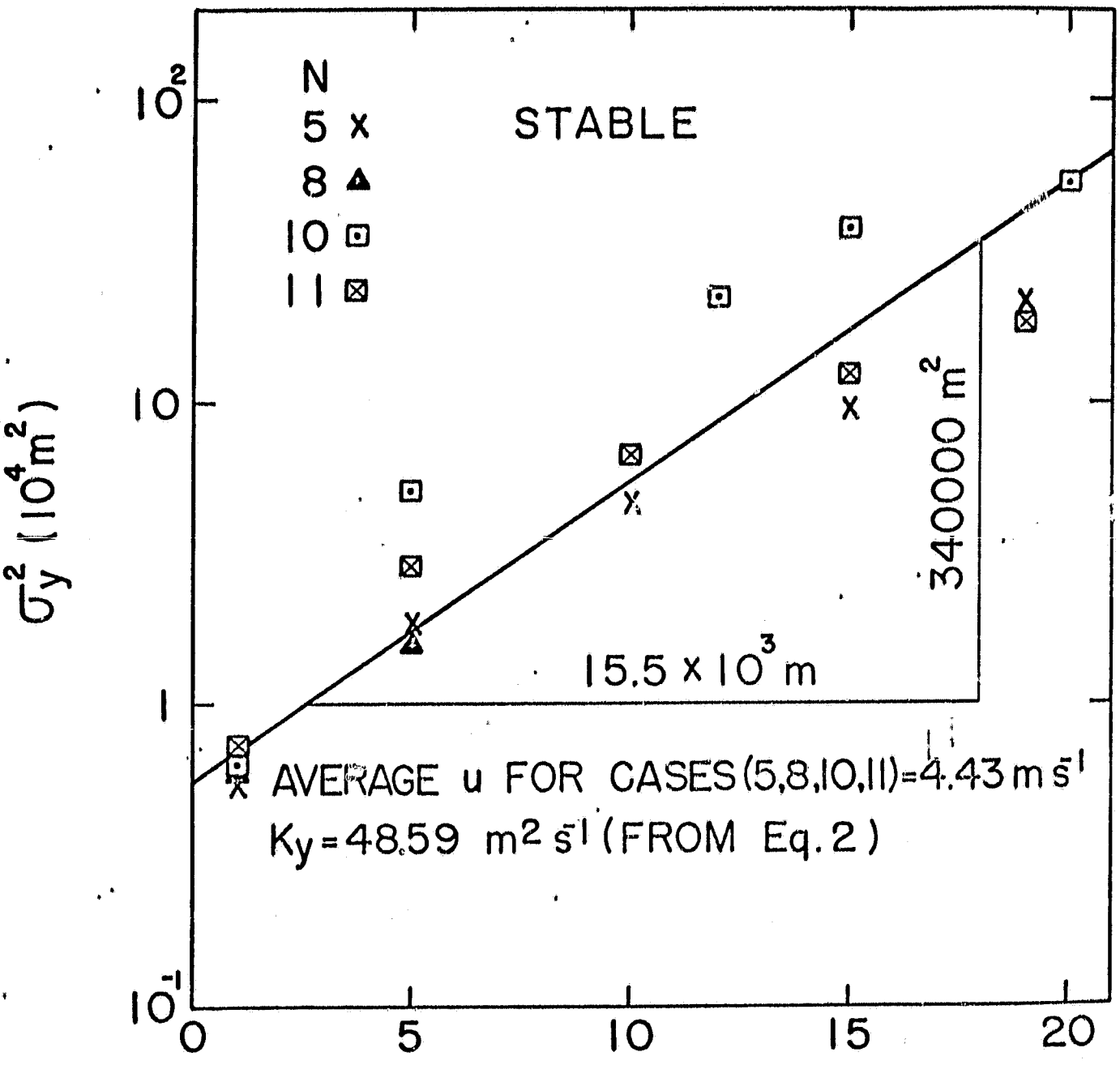

FIG. 16

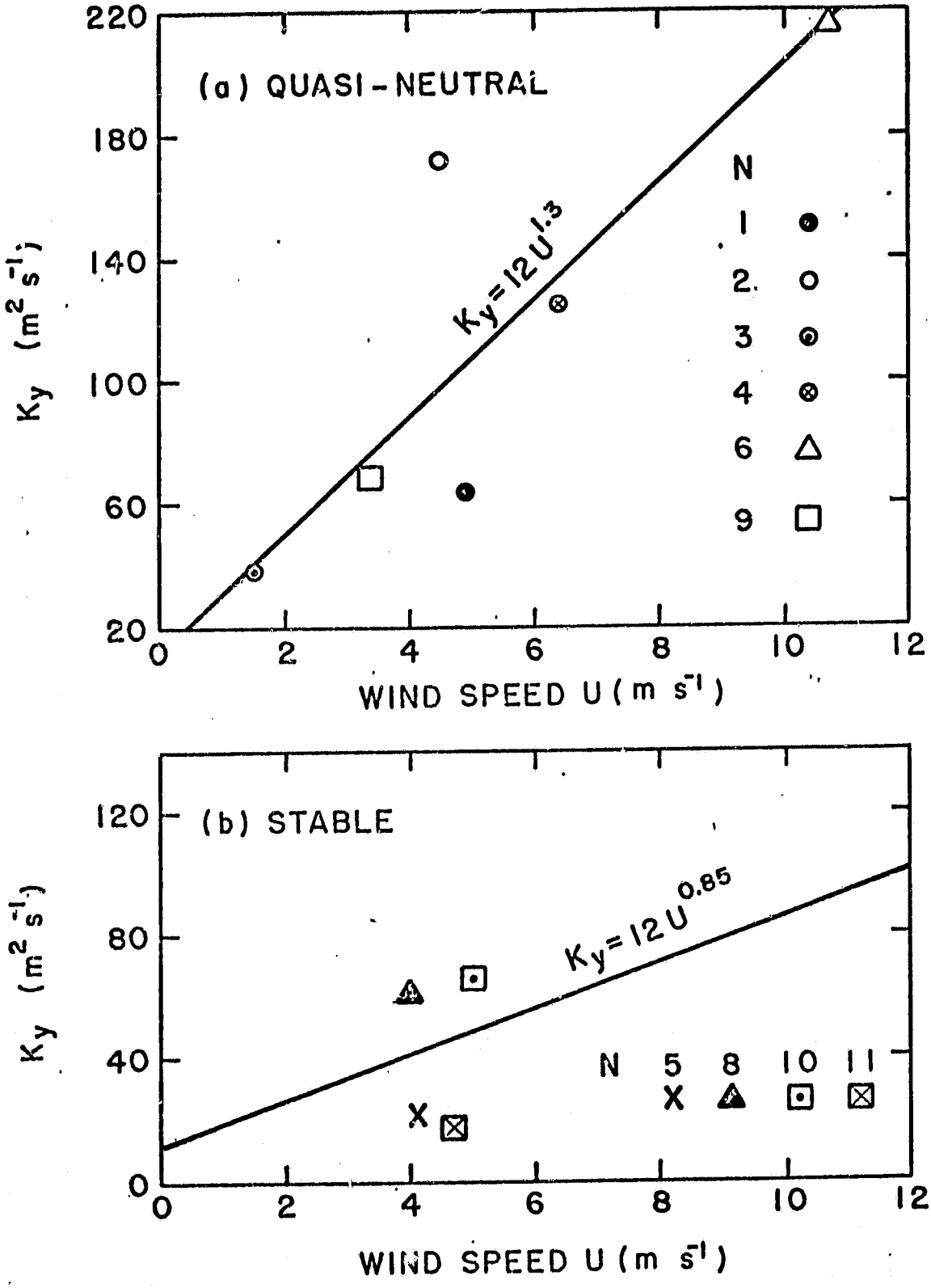

FIG. 17